Correlations, spin dynamics, defects: the highly-frustrated Kagomé bilayer

David Bono, Laurent Limot, Philippe Mendels, Gaston Collin, Nicole
Blanchard

HAL Id: hal-00004519
https://hal.archives-ouvertes.fr/hal-00004519

Correlations, spin dynamics, defects: the highly-frustrated Kagomé bilayer

David Bono,[*] Laurent Limot,[†] and Philippe Mendels[‡]

Laboratoire de Physique des Solides, UMR 8502, Université Paris-Sud, 91405 Orsay, France

Gaston Collin

Laboratoire Léon Brillouin, CE Saclay, CEA-CNRS, 91191 Gif-sur-Yvette, France

Nicole Blanchard

Laboratoire de Physique des Solides, UMR 8502, Université Paris-Sud, 91405 Orsay, France
(Dated: March 19, 2005)

The $SrCr_{9p}Ga_{12-9p}O_{19}$ and $Ba_2Sn_2ZnGa_{10-7p}Cr_{7p}O_{22}$ compounds are two highly-frustrated magnets possessing a quasi-two-dimensional Kagomé bilayer of spin $\frac{3}{2}$ chromium ions with antiferromagnetic interactions. Their magnetic susceptibility was measured by local Nuclear Magnetic Resonance and non-local (SQUID) techniques, and their low-temperature spin dynamics by Muon Spin Resonance. Consistent with the theoretical picture drawn for geometrically frustrated systems, the Kagomé bilayer is shown here to exhibit: (i) short range spin-spin correlations down to a temperature much lower than the Curie-Weiss temperature, no conventional long-range transition occurring; (ii) a Curie contribution to the susceptibility from paramagnetic defects generated by spin vacancies; (iii) low-temperature spin fluctuations, at least down to 30 mK, which are a trademark of a dynamical ground state. These properties point to a spin-liquid ground state, possibly built on Resonating Valence Bonds with unconfined spinons as the magnetic excitations.

I. INTRODUCTION

A. Highly frustrated magnets

Anderson's initial proposal of a Resonating Valence Bond (RVB) state was intended as a possible alternative for the Néel ground state of a triangular network with Heisenberg spins coupled by an antiferromagnetic interaction [1]. The RVB state, known also as a "spin-liquid" state because of the short-range magnetic correlations and spin fluctuations down to $T = 0$, was also proposed to explain the high-T_c behavior of cuprates [2] and, more recently, of the superconducting compound $Na_xCoO_2 \cdot yH_2O$ [3]. Although Anderson's conjecture was proven to be wrong for the triangular network [4], there is a growing consensus that the RVB state is the ground state of the so-called highly-frustrated networks [5, 6]. Like the triangular network, the magnetic frustration of these systems is exclusively driven by the triangular geometry of their lattice provided that spins are coupled through an antiferromagnetic (AFM) interaction. This is different from spin glasses, where frustration arises from the randomness of the magnetic interactions [7]. However, compared to a triangular network, these networks have a corner-sharing geometry, as in the two-dimensional Kagomé (corner sharing triangles, Fig. 1), the three-dimensional pyrochlore (corner sharing tetrahedras, Fig. 1), and the quasi-two-dimensional Kagomé bilayer (corner sharing triangles and tetrahedras, Fig. 2) lattices. The corner-sharing geometry introduces a "magnetic flexibility", thereby enhancing the frustration of these networks (thus the term "highly") and destabilizing the Néel order. A highly-frustrated network, and the experimental counterpart known as highly-frustrated magnet (HFM), is therefore an ideal candidate to possess a RVB ground state. Moreover, since HFMs are insulators, the experimental investigation of their ground state, and the related theoretical modelling, is greatly simplified by the absence of phenomena such as superconductivity, charge ordering or itinerant magnetism.

The original features of the ground state of the Heisenberg two-dimensional (2D) Kagomé network, which is the central issue of this paper, is already apparent through a *classical* description of their magnetism [8, 9, 10, 11], yielding a dynamical ground state with infinite degeneracy. More precisely, the "order by disorder" mechanism selects a coplanar spin arrangement in the ground state. However, the system can swap from one coplanar spin configuration to the other by a rotation of a finite number of spins, with no cost in energy. These zero-energy excitation modes, or soft modes, prevent a selection of one of the coplanar configurations [93] and constitute a low-energy reservoir of magnetic excitations. It results in a finite entropy per spin in the ground state, without, still up to now, any definitive conclusions on a possible long-range order, even at $T = 0$.

In a *quantum* description of the magnetism for Heisenberg spins $\frac{1}{2}$ on the Kagomé network, the magnetic

[*]Present address: Kamerlingh Onnes Laboratorium, Leiden University, P.O. Box 9504, 2300 RA Leiden, The Netherlands.
[†]Present address: Institut für Experimentelle und Angewandte Physik, Christian-Albrechts-Universität zu Kiel, D-24098 Kiel, Germany.
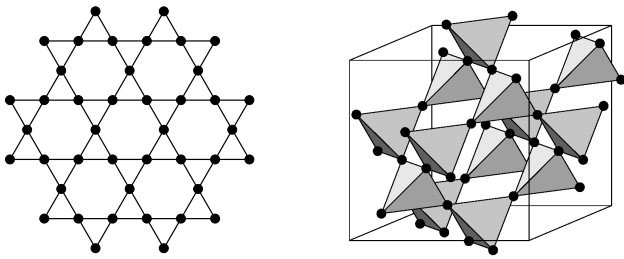[‡]Electronic address: mendels@lps.u-psud.fr

FIG. 1: The Kagomé (left) and the pyrochlore (right [12]) corner-sharing lattices. The coordinance of each site is 4 and 6, respectively.
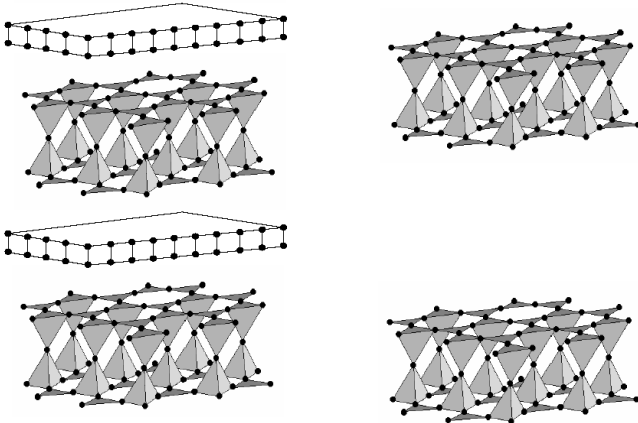

FIG. 2: Kagomé bilayers in SCGO (left) and in BSZCGO (right). Two different sites are present in the Kagomé bilayer lattice, one of coordinance 5, the other of coordinance 6. The magnetism of both compounds arises from the stacking of magnetically decoupled Kagomé bilayers, ensured in SCGO by the presence of the non-magnetic singlets and in BSZCGO by a large inter-bilayer distance.

designate by "disorder", may release the frustration and stabilize an original ground state [20, 21, 22, 23, 24, 25]. Experimentally, disorder is present in all HFMs and indeed causes cooperative phase transitions at low temperature, reminiscent of spin-glasses or AFM systems. This is typically observed in the jarosites Kagomé family, where the disorder is governed by spin anisotropy and by dipolar interactions [26] [95]. In the spin $\frac{1}{2}$ Kagomé $[Cu_3(titmb)_2(OCOCH_3)_6] \cdot H_2O$ compound, the competition between first- and second-neighbor interactions, respectively ferromagnetic and antiferromagnetic, yields an original ground state, with a double peak in the specific heat and plateaus in the magnetization under particular conditions [27]. In the $S = 1$ Kagomé staircase $Ni_3V_2O_8$, the competition between first and second neighbor interactions, combined to Dzyaloshinskii-Moriya interactions and spin anisotropy, produces a very rich field and temperature phase diagram [28]. In three dimensions (3D), dipolar couplings and interactions further than nearest neighbor yield long-range magnetic order at 1 K in the pyrochlore compound $Gd_2Ti_2O_7$ [29]. In $Y_2Mo_2O_7$, lattice distortions have been proposed to relieve the frustration in the ground state [30]. However, some samples, like the pyrochlore $Tb_{2-p}Y_pTi_2O_7$ [31, 32] or the spinel $ZnCr_2O_4$ [33], display spin dynamics down to very low temperature. Anyway, the high spin values and/or the 3D character of the frustrated geometry of these compounds remain far from the ideal Heisenberg Kagomé case we are dealing with. Along with the spin-liquid ground state of the ideal systems, the plethoric number of possible ground states in the presence of disorder (including the case of ferromagnetic interactions in the pyrochlore lattice, yielding the frustrated so-called "spin ice" ground state [34, 35], named so as it is equivalent to the order observed for hydrogen atoms in ice H_2O), constitutes one of the rich aspects of the HFMs.

B. SCGO and BSZCGO

Among all HFMs, the chromium-based spin $\frac{3}{2}$ Kagomé bilayer compounds $SrCr_{9p}Ga_{12-9p}O_{19}$ [SCGO(p)] [36] and the $Ba_2Sn_2ZnGa_{10-7p}Cr_{7p}O_{22}$ [BSZCGO(p)] [37] are the most likely candidates to possess a spin-liquid ground state. This is not surprising in view of the low spin value, 2D character and low level of disorder of these compounds compared to other HFMs. They are in fact an experimental realization of a quasi-2D Kagomé bilayer of spin $\frac{3}{2}$ chromium ions with antiferromagnetic interactions (Fig. 2). Moreover, the AFM interaction between nearest neighboring spins is dominated by a direct overlap exchange resulting in a coupling of $J \sim 40$ K (Sec. II). This coupling is almost two orders of magnitude larger than the typical disorder-related interactions, like single-ion anisotropy, estimated to 0.08 K [38, 39], dipolar interactions ~ 0.1 K, or next nearest neighbor interactions < 1 K. These compounds, however, always have a small amount of substitutional disorder, since a Cr-coverage

ground state is disordered [11]. It is predicted to be RVB-like, built on a macroscopic number of singlet states [13, 14]. If any, a gap between the ground state and the first triplet state is expected to be fairly small, of the order of $J/20$ [15], where J is the AFM interaction between nearest neighbor spins [94]. Most strikingly and similar to the classical case, the corner-sharing geometry and the half-integer spins lead to an exponential density of low-lying singlet excitations [16], with energies smaller than the gap, and to a non-zero entropy per spin at $T = 0$ [17]. The same conclusions seem to emerge for the AFM pyrochlore lattice [18]. The nature of the magnetic excitations, possibly unconfined spinons, is still an open question [17, 19].

As a major drawback, every additional contribution to the nearest-neighbor AFM interaction, such as next-nearest-neighbor interactions, dipolar interactions, anisotropy, Dzyaloshinskii-Moriya interactions, lattice distortions or magnetic defects generated by the presence of magnetic impurities or spin vacancies, all of which we
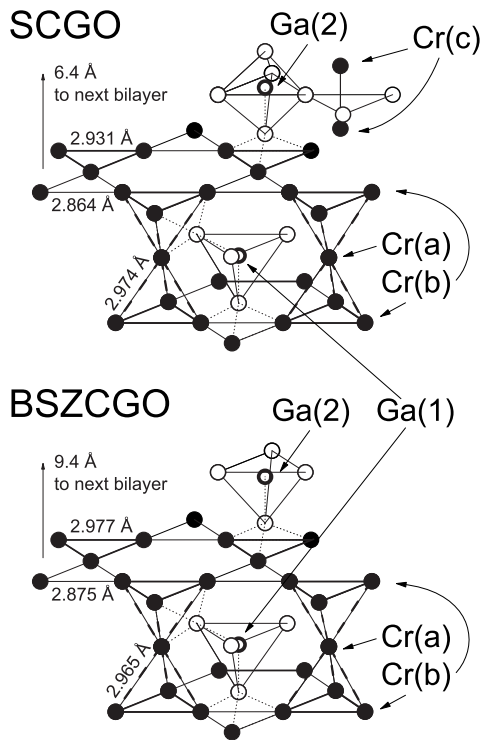
FIG. 3: Cr^{3+} network of SCGO and BSZCGO with their oxygen ($\bigcirc$) environments, along with the two Ga^{3+} sites. The dotted lines represent some of the Ga-O-Cr hyperfine coupling paths.

higher than $p = 0.95$ and $p = 0.97$ cannot be reached in SCGO(p) [40] and in BSZCGO(p) [41], respectively. Hence there are always at least some percent of the magnetic Cr^{3+} ions which are substituted with non-magnetic Ga^{3+} ions. These low amounts of spin vacancies, and the related magnetic defects that they produce, turn out to be insufficient to destroy the spin-liquid behavior of the ground state. We will show that local techniques like Nuclear Magnetic Resonance (NMR) and Muon Spin Relaxation (μSR) are the most suited to probe frustration-related properties in these systems, since they can bypass the magnetic contribution of these defects.

Figure 3 presents a simplified chemical structure for the ideal $p = 1$ unit cell of SCGO and of BSZCGO, highlighting the chromium Kagomé bilayers [96]. As it can be seen, BSZCGO is a pure Kagomé bilayer, on the contrary of SCGO where there are two additional chromium sites, labelled Cr(c), between the bilayer. These pairs of Cr-spins are coupled by an AFM exchange constant of 216 K with a weak coupling to the Kagomé bilayers (~ 1 K) [42]. They form an isolated singlet at low temperatures, and the resulting susceptibility is negligible at $T \lesssim 50$ K compared to the susceptibility of the Kagomé bilayer in a pure compound. Moreover, the Ga/Cr substitutions are substoechiometric on these sites (see Sec. II C 3). The full crystal structure is obtained by the stacking of the unit cells presented in Fig. 3. The magnetism of both
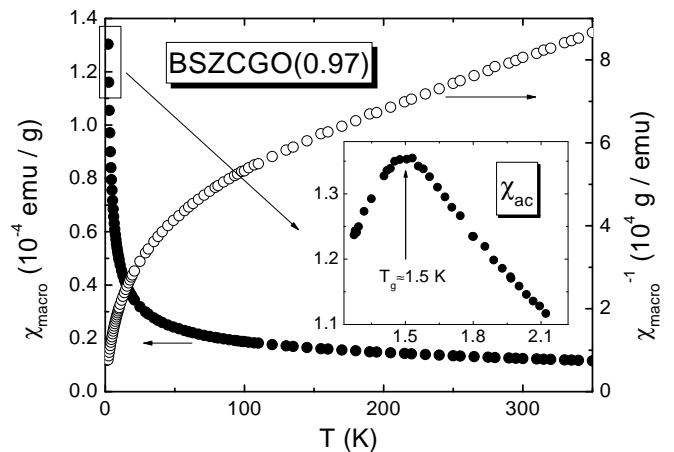

FIG. 4: Macroscopic static susceptibility $\chi_{macro}(T)$ of BSZCGO(0.97) measured with a SQUID under 100 G (left scale) and $\chi_{macro}^{-1}(T)$ (right scale). Inset : ac susceptibility (78 Hz) below 2 K focusing on the spin-glass-like transition (T_g).

compounds arises by magnetically decoupled Kagomé bilayers, ensured in SCGO by the presence of the non-magnetic singlets at low temperature (only weakly affected by the Ga/Cr substitution, see Sec. II C 3), and in BSZCGO by the large interbilayer distance of 9.4 Å (in SCGO of 6.4 Å). These compounds can therefore be considered as ideal two-dimensional systems.

Figure 4 shows the typical macroscopic susceptibility χ_{macro} in these compounds. The linearity of χ_{macro}^{-1} at high temperature and the extrapolation of this line to $\chi_{macro}^{-1} = 0$ to a negative temperature is typical of AFM interactions and gives an order of magnitude of the Curie-Weiss temperature $\theta_{CW} = zS(S + 1)J/3$ (600 K and 350 K for SCGO and BSZCGO). However, contrary to the case of "conventional" antiferromagnets [43], no kink is evidenced in χ_{macro} around θ_{CW}. This is actually one of the common signatures of the frustration in HFMs [5]: the magnetic correlation length cannot increase because of frustration, and mean field theory remains valid for $T \sim \theta_{CW}$. At low temperature, a spin-glass-like transition occurs in both systems, around a freezing temperature $T_g \sim 3$ K in SCGO(p) and 1.5 K in BSZCGO(p) (Fig. 5).

However, unlike in other HFMs, the spin-glass transition is unconventional. In fact, in *conventional 3D spin glasses*, the nonlinear susceptibility diverges at T_g, the specific heat is proportional to T at low temperature, and T_g is proportional to the number of defects. In the *Kagomé bilayers*, however, (i) the nonlinear susceptibility diverges at T_g [44], but T_g increases when the number of spin vacancies decreases (Fig. 5), indicating that the freezing is related to an intrinsic property of the frustrated bilayer. (ii) The specific heat is proportional to T^2, as in *AFM 2D long-range ordered systems*. Its unusual large value at low temperature unveils a high density of low-lying excitations [37, 44], and its insensitivity
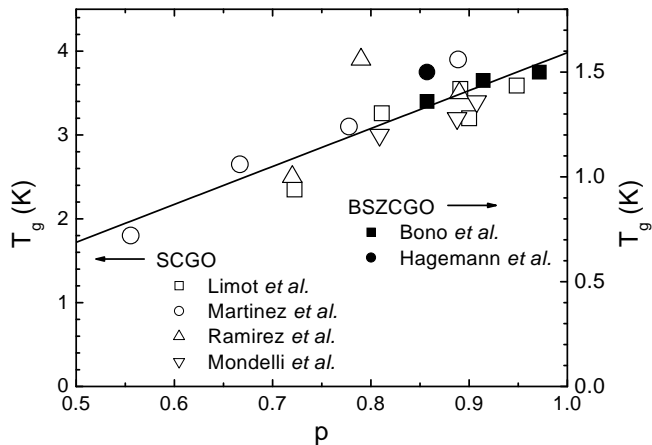
FIG. 5: Collection of spin-glass-like transition temperatures T_g for SCGO and for BSZCGO versus Cr-concentration p (our data and from Ref. 37, 38, 50, 51). The line is a guide to the eye.

to an external magnetic field suggests a large contribution from singlet excitations, which is one of the most striking features predicted for the $S = \frac{1}{2}$ Kagomé lattice [45, 46, 47]. (iii) Magnetic fluctuations and short-range correlations, consistent with a 2D magnetic network, are encountered at low temperature [48, 49]. The Kagomé bilayers therefore combine properties of 3D spin glasses, 2D AFM ordering, 2D fluctuating magnetic states and original properties expected in $S = \frac{1}{2}$ Kagomé systems.

Given these two temperature scales of the macroscopic susceptibility, θ_{CW} and T_g, Ramirez proposed the definition of a "frustration ratio", $f = \theta_{CW}/T_g$, with $f > 10$ in all HFMs [52]. The Kagomé bilayers SCGO and BSZCGO respectively display $f \sim 150$ and 230 [41], the largest ratios reported so far in compounds where the frustration is driven by corner sharing equilateral triangles [5]. The large frustration, the Heisenberg spins along with the low disorder, make them the archetypes of HFM and maybe the best candidates for a RVB spin-liquid ground state.

We present a review of the magnetic properties of SCGO(p) and BSZCGO(p) *powder samples*, which covers a large range of Cr-concentration p. The comparison between samples of different concentration allows to identify the frustrated and disorder-related magnetic properties of the Kagomé bilayer. Through local probes it is then possible to determine the true nature of the bilayer's static susceptibility (by NMR), as well as the bilayer's low-temperature dynamics and ground state magnetic excitations (by μSR). The outline of the paper is as follows. Section II is dedicated to the susceptibility of the Kagomé bilayer. It is shown that the susceptibility of the bilayer of SCGO and of BSZCGO can be accessed directly through gallium NMR experiments [40, 41, 53, 54, 55, 56]. Both susceptibilities exhibit a maximum in temperature at $T \sim 40$ K $\sim J$ and decrease below this maximum down to at least $J/4$. This be-

havior indicates that short-range magnetic correlations persist at least down to 10 K, consistent with the existence of a small spin gap. The comparison of the Kagomé bilayer's susceptibility with χ_{macro} shows that the spin vacancies of the bilayer generate paramagnetic defects responsible for the low-temperature Curie upturn observed in the macroscopic susceptibility (both systems have also extra Curie contributions, coming from broken Cr(c) spin-pairs in SCGO and from bond length distribution in BSZCGO). Section III is dedicated to the μSR study of the low-temperature spin dynamics of these HFMs [49, 56, 57, 58]. It is shown, that magnetic excitations persist down to at least 30 mK (the lowest temperature that could be accessed). This temperature sets an upper limit for the value of a spin gap. A qualitative and quantitative analysis of the data shows that these excitations are possibly coherent unconfined spinons of a RVB ground state. The energy scale T_g would correspond then, in this phenomenological approach, to the signature of this coherent resonating state. A summary and concluding remarks can be found in Sec. IV.

II. FRUSTRATED VS. DISORDER-RELATED SUSCEPTIBILITY

A. Gallium NMR in SCGO and BSZCGO

The NMR experiments were performed on ^{69}Ga ($^{69}\gamma/2\pi = 10.219$ MHz/T, $^{69}Q = 0.178 \times 10^{-24}$ cm^2) and ^{71}Ga ($^{71}\gamma/2\pi = 12.983$ MHz/T, $^{71}Q = 0.112 \times 10^{-24}$ cm^2) nuclei in SCGO and BSZCGO using a $\frac{\pi}{2}$-τ-π spin echo sequence, where γ and Q are, respectively, the gyromagnetic ratio and the quadrupolar moment of the nuclei. The gallium ions are located on two distinct crystallographic sites, labelled Ga(1) and Ga(2) in Fig. 3. As pointed out in Ref. 40, 41, 53, 56, the interest of Ga NMR lies in the coupling between gallium nuclei with their neighboring magnetic Cr^{3+} ions through a Ga-O-Cr hyperfine bridge (Fig. 3). In particular, the ^{69,71}Ga(1) nuclei are exclusively coupled to the Cr^{3+} ions of the Kagomé bilayer: to nine chromium ions of the upper and lower Kagomé layers (labelled Cr(b) in Fig. 3), and to three chromium ions in the linking site in between the two Kagomé layers (labelled Cr(a) in Fig. 3). Through the NMR of Ga(1), it is possible to probe locally the magnetic properties of the Kagomé bilayers of both HFMs. This is the central topic of the NMR study presented in this paper.

Before going any further, we briefly recall some relationship between the contribution of each gallium nucleus to the Ga(1) NMR line and its local magnetic environment in order to underline what can be exactly probed through Ga(1) NMR. We suppose first that the susceptibility in the Kagomé bilayer varies from chromium site to chromium site and label it, in a generic manner, by χ. A Ga(1) at site i will contribute to the NMR spectrum at a position depending upon the number of the nearest

TABLE I: Quadrupole parameters for the ^{71}Ga sites in SCGO [40, 53] and in BSZCGO [41]. Notice that $^{69}\nu_Q = (^{69}Q/^{71}Q)\nu_Q \approx 1.59^{71}\nu_Q$. Quadrupole effects are therefore more pronounced for the ^{69}Ga isotope than for the ^{71}Ga.

	Ga site	$^{71}\nu_Q$ (MHz)	η
SCGO	Ga(1)	2.9(2)	0.005(6)
	Ga(2)	20.5(3)	0.050(35)
BSZCGO	Ga(1)	3.5(1.0)	0.60(15) [a]
	Ga(2)	12.0(5)	0.04(3)

[a] Determined using point charge simulation.

neighbors (NN) occupied chromium sites and their susceptibility χ. This corresponds to the shift $K^{(i)}$ in the NMR spectrum for a gallium at site i

$$K^i = \sum_{\text{occupied NN Cr}(a,b)} A\chi \ , \qquad (1)$$

where A is the hyperfine constant (the chemical shift is neglected here). The average shift, K, of the NMR line, is simply related to the average $\overline{K^i}$ over all the gallium sites. Hence, it is practically proportional to the average susceptibility χ_{Kag} of the Kagomé bilayer. On the other hand, the distribution of K^i around K defines the magnetic width of the Ga NMR line and reflects the existence of a distribution of χ. As we show in the following sections, the NMR width probes a susceptibility related to disorder in BSZCGO and in SCGO.

Along with this hyperfine interaction, the ^{69,71}Ga Hamiltonian in SCGO and in BSZCGO has a quadrupolar contribution. The quadrupole interaction of gallium nuclei in both SCGO and BSZCGO is a consequence of the coupling of the nucleus to the electric field gradient (EFG) produced by the surrounding electronic charges. Following the usual notations, the nuclear Hamiltonian may be expressed as

$$\mathcal{H} = -\gamma\hbar\mathbf{I}\left(\bar{1} + \bar{K}\right)\mathbf{H_0} + \frac{h\nu_Q}{6}\left[3I_z^2 - I^2 + \eta\left(I_x^2 - I_y^2\right)\right] \ , \qquad (2)$$

where $\mathbf{H_0}$ is the applied magnetic field, ν_Q the quadrupolar frequency and $0 \leq \eta \leq 1$ the asymmetry parameter. The principal axes of the shift tensor $\bar{K}$ are collinear with the direction of the nuclear spin operators I_x, I_y and I_z.

As shown in Fig. 3 the gallium sites of both HFMs have different crystallographic environments. Some simple arguments can be used to anticipate differences concerning their spectra (Tab. I):

(i) The Ga(1) sites of both HFMs have a nearly-tetrahedral oxygen environment. Given this nearly-cubic symmetry, the EFG is small, i.e. ν_Q is small. However, whereas the Ga(1) site of SCGO is only occupied with Ga^{3+} ions, the Ga(1) site of BSZCGO is randomly occupied either by Zn^{2+} or by Ga^{3+} ions. As a consequence, point charge simulations of the EFG on the Ga(1) site of BSZCGO show that there is a large distribution of η and ν_Q, contrary to the Ga(1) of SCGO.

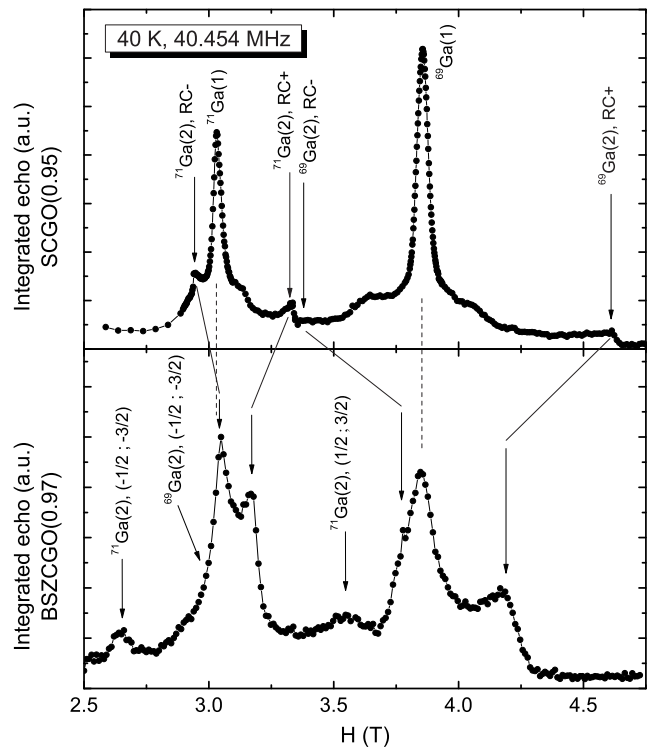FIG. 6: Comparison of the ^{69,71}Ga NMR spectra in SCGO and BSZCGO obtained by sweeping the field with a constant frequency $\nu_l \approx 40$ MHz, at $T = 40$ K. The arrows point the quadrupolar singularities for the Ga(1) and Ga(2), respectively located inside and outside the bilayers (Fig. 3). "CL" points the central line ($\frac{1}{2} \leftrightarrow -\frac{1}{2}$ transition) singularities. The continuous and dashed lines show the shift of the in-range singularities of the Ga sites, from one system to the other. We cannot identify the first order satellites of the Ga(1) in BSZCGO on this spectrum.

(ii) The Ga(2) site of SCGO is surrounded by a bi-pyramid of 5 oxygen ions, whereas the Ga(2) of BSZCGO lies in an oxygen-elongated tetrahedra. Both environments have no cubic symmetry which yields a large quadrupolar frequency. For this site, point charge simulations yield a ν_Q twice larger in SCGO than in BSZCGO.

(iii) The ratio Ga(1):Ga(2) is 2:1 in SCGO, whereas it is 1:2 in BSZCGO. Consequently, the relative spectral weight of the Ga(1) and Ga(2) sites will be opposite in the two compounds.

An extensive study of the ^{69,71}Ga NMR spectra in SCGO was presented in Ref. 40, 53. It allowed to identify the NMR lines and to extract the parameters of the nuclear Hamiltonian, among them the quadrupolar parameters given in Tab. I. It was shown that the Ga NMR spectrum of both isotopes is the sum of the Ga(1) and Ga(2) sites, plus a small extra contribution related to the presence of the non-stoichiometric gallium substituted on the chromium sites (labelled Ga(sub) in Fig. 8). A similar analysis allowed to identify the NMR lines in BSZCGO, and to determine the related parameters of the nuclear
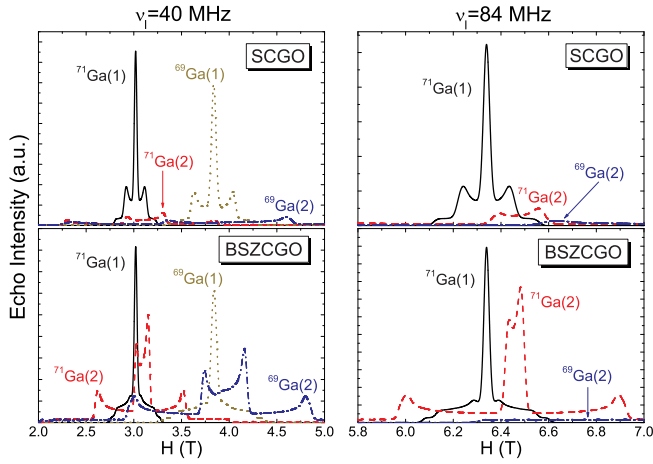
FIG. 7: Quadrupolar powder pattern simulations for both sites and isotopes with the parameters of Tab. I, for frequencies $\nu_l = 40$ MHz (left) and 84 MHz (right) in SCGO and BSZCGO. The area of each contribution is obtained considering the stoichiometry of each site in the samples and the natural abundance of each isotope. The full NMR spectra are obtained by adding all the contributions (not shown).

Hamiltonian [41], also listed in Tab. I.

Neglecting the Ga-substituted sites, the Ga NMR spectrum displays four sets of lines corresponding to the two isotopes distributed on both Ga(1) and Ga(2) sites. In a powder sample, as used here, for a given site and a given isotope, the line shape results from the distribution of the angles between the magnetic field and the EFG principal axes. This yields singularities rather than well defined peaks (the so-called powder line shape), as in the Ga NMR spectra of SCGO(0.95) and of BSZCGO(0.97) presented in Fig. 6.

Powder-pattern simulations for two different r.f. frequencies ($\nu_l = 40$ MHz and 84 MHz) are presented in Fig. 7, using the parameters of Tab. I. They perfectly agree with the experimental NMR spectra and clearly show that the BSZCGO spectrum is more intricate than the SCGO one, because of the more pronounced quadrupolar contribution. This is probably the reason why the Ga(sub) line cannot be resolved in BSZCGO, contrary to SCGO.

Most of the SCGO data were acquired in a field-sweep spectrometer with a r.f. frequency $\nu_l \approx 40$ MHz, because then the ^{69,71}Ga(1) NMR lines can be isolated, as shown in Fig. 7 [40]. At high temperatures (Fig. 8a), the NMR line shape remains unaltered and shifts with decreasing temperature. At low temperature ($T < 50$ K), the line broadens with decreasing temperature (Fig. 8b). The ^{69,71}Ga(1) shift is still qualitatively visible down to 5 K, where the Ga NMR signal is lost (see below). Fits of the low-temperature spectra (using a convolution of a high-temperature unbroadened spectrum with a Gaussian) allow to extract quantitatively the shift and the width of the NMR lines for all the samples studied ($0.72 \leq p \leq 0.95$). All display similar shifts with temperature, but different broadening, the line shape increasing with Ga/Cr substitution at a given temperature [40].

In the case of BSZCGO, it can be seen from Fig. 7 that it is advantageous to work at a frequency higher than 40 MHz, in order to isolate the Ga(1) contribution [97]. Field-sweep ^{71}Ga NMR experiments were performed at a r.f. frequency $\nu_l \approx 84$ MHz. At high temperature (Fig. 9a), a ^{71}Ga(1) shift is evidenced similar to the one in SCGO [98]. At low temperature, the ^{71}Ga(1) and ^{71}Ga(2) lines broaden and start to overlap. However, the two lines can be resolved by exploiting the different transverse relaxation times T_2 of the two gallium sites ($T_{2,Ga(1)} \sim 20$ μs, $T_{2,Ga(2)} \sim 200$ μs). The first step consists in using a large time separation between the two r.f. pulses ($\tau = 200$ μs) in order to eliminate the Ga(1) contribution. The isolated Ga(2) line is extracted using a gaussian convolution of the quadrupolar powder pattern. In the second step, a short time separation is employed between the pulses ($\tau \approx 10$ μs) so that the Ga(1) contribution is recovered. The Ga(1) line is finally isolated by subtracting the long τ spectrum corrected in intensity to account for the shorter time separation employed [99]. Such a procedure can be employed down to 10 K. The width and the shift of the Ga(1) line can then be extracted from a fit using a $^{71}\nu_Q = 3.5$ MHz quadrupolar powder pattern convoluted by a gaussian line shape, and are little affected by the uncertainty on $^{71}\nu_Q$. The ratio between the intensities of the Ga(2) and Ga(1) lines (integrated area below the lines) was found to stay close to 2 down to 10 K, in agreement with the 2:1 stoichiometric ratio for the Ga(2) and Ga(1) sites of BSZCGO.

The temperature dependence of the intensity of the ^{71}Ga(1) NMR line, which corresponds to the number of detected ^{71}Ga(1) nuclei, is presented in Fig. 10 for SCGO. A similar trend is observed in BSZCGO, with larger error bars due to the preponderant Ga(2) contribution. As temperature decreases the spin dynamics slows down, and results in a decreasing longitudinal relaxation time T_1 (see Sec. III), hence in a progressive loss of the NMR signal below 15 K. Such a wipeout is reminiscent of the one observed in spin-glasses at temperatures near T_g [59]. However, contrary to spin-glasses where ultimately the signal is recovered below T_g, there is no evidence for such a recovery in SCGO, nor in BSZCGO.

B. Susceptibility of the Kagomé bilayer

The Kagomé bilayer susceptibility χ_{Kag} is probed through the shift K of the ^{69,71}Ga(1) NMR lines [40, 41, 54], presented in Fig. 12 for the purest samples of both systems in a temperature range displaying no significant loss of intensity ($T \gtrsim 10$ K). The shift (and χ_{Kag}) increases when the temperature decreases up to 45 K, where a maximum is reached, and then decreases again as the temperature is lowered. This behavior is common to both systems and is field- and dilution-independent [54]. Most importantly, it is quite clear from Fig. 11 that
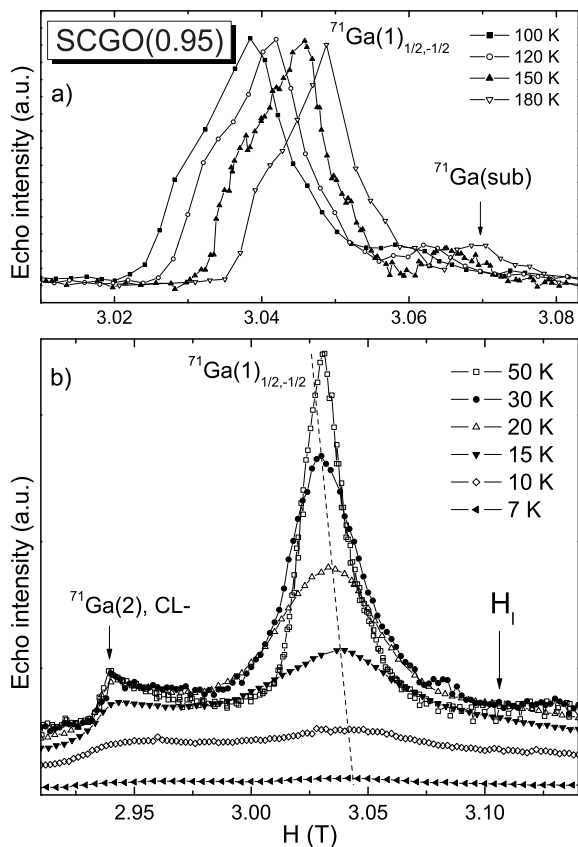
FIG. 8: ^{71}Ga spectra in SCGO ($H_l = 2\pi\nu_l/^{71}\gamma$). a) High temperature. The ^{71}Ga(2) contribution appears as a flat background in this field range. b) Low temperature, lines are broadened. The ^{71}Ga(2) contribution remains flat at the position of the ^{71}Ga(1) line, which shifts to higher fields in this temperature region when the temperature decreases.

FIG. 9: ^{71}Ga spectra in BSZCGO. a) High temperature. The ^{71}Ga(2) first order quadrupolar contribution appears as a flat background in this field range at the ^{71}Ga(1) line position. b) Low temperature, lines are broadened. ○ and □ are the short τ and the rescaled long τ spectra respectively. △ is for the Ga(1) contribution, given by their subtraction. The dotted arrows point at the center of the Ga(1) line, which shifts to higher fields when T decreases. Continuous (dashed) lines are gaussian broadened ^{71}Ga(1) [^{71}Ga(2)] quadrupolar powder pattern simulation, with $\nu_Q = 3.5$ MHz (12 MHz) and $\eta = 0.6$ ($\eta = 0.04$).

there is a discrepancy between the low-temperature behavior of χ_{Kag} and of χ_{macro}. Instead of a maximum, the susceptibility probed by SQUID measurements follows a Curie-like law at low temperature. This establishes that χ_{macro} is a two-component susceptibility [100], resulting from the sum of the Kagomé bilayer's susceptibility and, as evidenced in Sec. II C, of a susceptibility related to magnetic defects (χ_{def}):

$$\chi_{\mathrm{macro}} = \chi_{\mathrm{Kag}} + \chi_{\mathrm{def}} \cdot \quad (3)$$

Concerning the high-temperature ($T \geq 80$ K) behavior of K, a phenomenological Curie-Weiss law, $K = C_{\mathrm{NMR}}/(T + \theta_{\mathrm{NMR}})$, is an accurate fit, yielding $\theta_{\mathrm{NMR}} = 440 \pm 5$ K and 380 ± 10 K, respectively for SCGO(0.95) and BSZCGO(0.97). The "Curie-Weiss" constant C_{NMR} found from the fit is 20% larger in SCGO than in BSZCGO, which indicates that hyperfine couplings are stronger in SCGO, likely because of the shorter Ga-O-Cr bonds (Fig. 3). Although very commonly employed to extract information from the HFMs susceptibility, this phenomenological law is a rather crude approximation, since the linear behavior of the inverse of the suscepti-
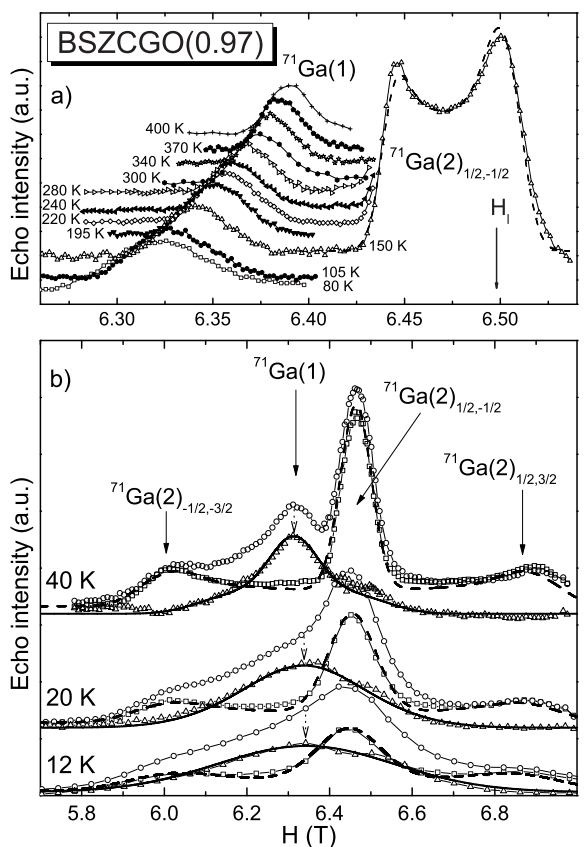
bility is expected to hold, within a mean field approach, only when $T \gtrsim 2\theta_{\mathrm{NMR}}$, which is not the case here. From θ_{NMR}, one can therefore only grossly estimate the coupling constants J of the Kagomé bilayers. In the absence of any prediction for $S = \frac{3}{2}$, we used the high temperature series expansion of χ_{Kag}, derived for a $S = \frac{1}{2}$ Kagomé lattice, to correct θ_{NMR} by a factor 1.5 [60]. The coupling constant is finally extracted from the mean-field relation $\theta_{\mathrm{NMR}} = 1.5zS(S + 1)J/3$. The coordinance is $z = 5.14$ and corresponds to the average number of nearest neighbors for a chromium ion of the bilayer. The couplings then read $J = 45$ K and 40 K for SCGO and BSZCGO, respectively. These values are consistent with the couplings observed in other chromium-based compounds [61, 62], and they indicate that the Cr-Cr AFM interaction stems from the direct overlap between orbitals of neighboring chromium ions, rather than from
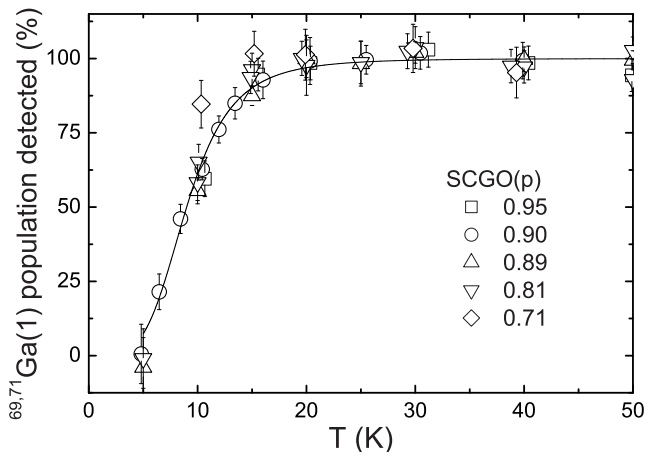
FIG. 10: NMR signal intensity in several SCGO(p) samples. A loss of ^{69,71}Ga sites is observed for $T \lesssim 5T_g$ (~ 16 K). The line is a guide to the eye.
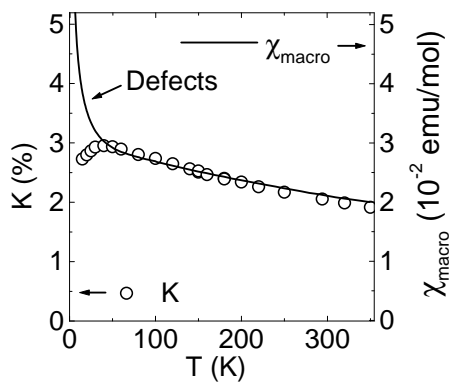

FIG. 11: K (left) and χ_{macro} (right) for SCGO(0.95). The NMR shift and the SQUID susceptibility do not follow exactly the same law at high temperature, since χ_{macro} also probes the susceptibility of the Cr(c)-Cr(c) spin pairs of SCGO (a detailed analysis can be found in Fig. 13 of Ref. 40).

an oxygen-mediated superexchange coupling. A direct interaction results in a coupling J very sensitive to the Cr-Cr distance (d), and follows a phenomenological law of [40]

$$\delta J / \delta d = 450 \text{ K/Å} . \qquad (4)$$

The slightly stronger coupling found in SCGO compared to BSZCGO results then, following this viewpoint, from the shorter Cr-Cr bond lengths of its Kagomé bilayer (Fig. 3).

We now turn to the low-temperature behavior of χ_{Kag}, and in particular we discuss the maximum around 45 K. The first possible interpretation of this maximum is the existence of a spin gap. Such a gap Δ is an important issue for the Kagomé bilayer, since it would be the signature of the existence of a singlet ground state, found in the theoretical quantum description of a $S = \frac{1}{2}$ Kagomé layer [15]. Its value is predicted to be $\Delta = J/20$, and
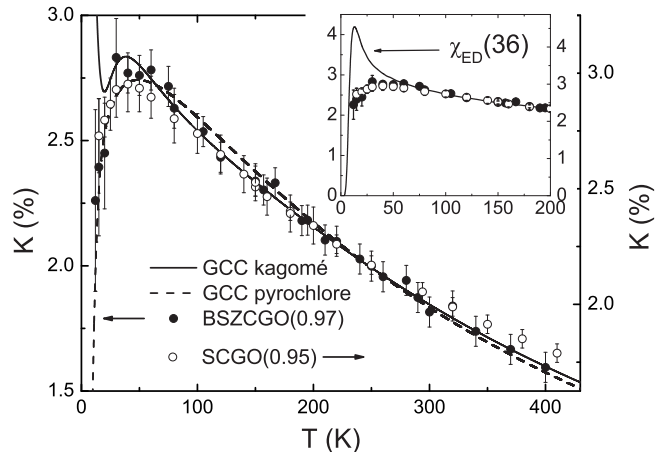

FIG. 12: Shift of the ^{71}Ga(1) line in SCGO and BSZCGO. Lines are GCC calculations (see text). Inset: Full scale down to 0. The line is the 36 spin $S = \frac{1}{2}$ cluster calculation mentioned in the text (χ_{ED}).

should be of the same order for higher spins [101]. Since Ga NMR cannot access lower temperatures than 10 K, which corresponds for SCGO and BSZCGO to $J/4$, we cannot conclude whether the maximum in temperature is related to a gap. From an experimental point of view, its observation would require temperatures $T < \Delta$ in order to observe the exponential decrease predicted for the susceptibility [47]. In the inset of Fig. 12, we compare our experimental data to the susceptibility computed with exact diagonalization on a 36 spin $S = \frac{1}{2}$ Kagomé cluster [19]. We see that the position of the predicted maximum does not match the experimental one. Also, the sharp peak of the susceptibility of the calculation is not seen in χ_{Kag}. Clearly, larger cluster sizes and the Kagomé bilayer geometry are needed for a better comparison to the NMR data. For the time being, it may be safely concluded, that the behavior of the NMR shift, hence of χ_{Kag}, is only consistent with a spin gap smaller than $J/10$.

Rather than the signature of a gap, the maximum in χ_{Kag} was assigned in Ref. 54 to the signature of a moderate increase of the spin-spin correlations of the Kagomé bilayer which, however, must remain short ranged given the absence of any phase transition. This conclusion was confirmed by neutron measurements on SCGO for temperatures ranging from 200 K down to 1.5 K [63], and by susceptibility calculations performed on the Kagomé and the pyrochlore lattices with Heisenberg spins, in which the spin-spin correlation length is kept of the order of the lattice parameter [64]. These calculations, using the so-called "generalized constant coupling" method (GCC) [64], consists in computing the susceptibility of isolated spin-clusters with zero-magnetic moments (triangles for the Kagomé and tetrahedras for the pyrochlore) and in coupling these clusters following a mean field approach. In the case of the pyrochlore lattice, an exponential decrease of the susceptibility is obtained at low tempera-

ture. In this case, the ground state of a cluster is non magnetic and the spin gap is between the $S = 0$ ground state and the magnetic $S = 1$ excited states. In the case of the Kagomé lattice, the ground state of the triangle is magnetic ($S_{\text{total}} = \frac{1}{2}$) which gives rise to the non-physical divergence in the susceptibility as $T \to 0$, due to the choice of a particular cluster [64]. The GCC simulations for the $S = \frac{3}{2}$ Kagomé and pyrochlore lattices, in between which the Kagomé bilayer's susceptibility is expected to lie, are presented in Fig. 12. As shown, they agree with the data down to $T = 40$ K $\ll \theta_{\text{NMR}}$, yielding a maximum and a behavior around the maximum in agreement with the experimental findings. From the simulations, the values of θ_{CW} are 260 K for SCGO(0.95) and 235 K for BSZCGO(0.97), which correspond to $J = 40$ K and $J = 37$ K, close to the previous values obtained through the high-temperature Curie-Weiss law.

In conclusion, the GCC computation fits quite well the data down to $T \sim J \ll \theta_{CW}$, where $J \approx 40$ K. It only shows that the strongest underlying assumption of this cluster mean-field approach is relevant, i.e., the spin-spin correlation length is of the order of the lattice parameter, which prevents any magnetic transition to a long range ordered state.

C. Defect-related susceptibility

In this section, we focus on the defects contribution to the susceptibility. The NMR linewidth and the SQUID data at low temperature show that the paramagnetic susceptibility χ_{def} observed in χ_{macro} comes from the dilution of the Kagomé bilayer and from other kinds of defects, namely the Cr(c) pairs in SCGO and bond defects in BSZCGO. The Ga(1) NMR width not only enables to evidence that the vacancy of a spin on the network, i.e. the dilution, generates a paramagnetic defect, but also allows to shed light on the more fundamental question concerning the extended nature of the defects. We first present the experimental facts concerning the magnetic defects, as measured quantitatively through the NMR linewidth and the SQUID susceptibility χ_{macro} and then elaborate on their nature in both compounds.

1. NMR linewidth

The Ga(1) NMR linewidth of SCGO and of BSZCGO was measured for various Cr-concentrations p. Figure 13 presents the typical p-dependence of the linewidth in both samples — in the figure, only for SCGO. In agreement with the qualitative presentation of the raw spectra in Sec. II A, the width increases as temperature drops and is well described by $1/T$ Curie law (lines in Fig. 13). It is very sensitive to the lattice dilution, similarly to the low-temperature behavior of χ_{macro} (Fig. 16), but differs from the NMR shift. The perfect scaling of the widths of the two ^{69,71}Ga(1) isotopes (e.g. SCGO(0.95) in Fig. 13)
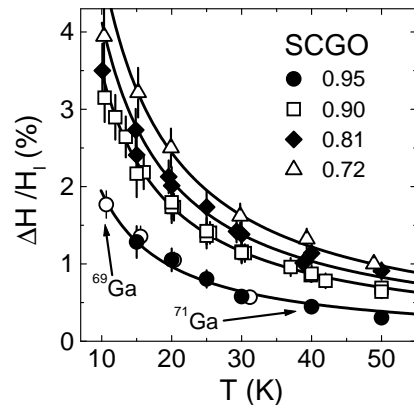
FIG. 13: Ga(1) NMR width versus temperature for SCGO samples of different Cr-concentration. The width ΔH is normalized by the reference field $H_l = \nu_l / ^{69,71}\gamma$ to superimpose the results from the two gallium isotopes (as explicitly shown for $p = 0.95$). The solid lines are $\propto 1/T$ Curie-like fits.
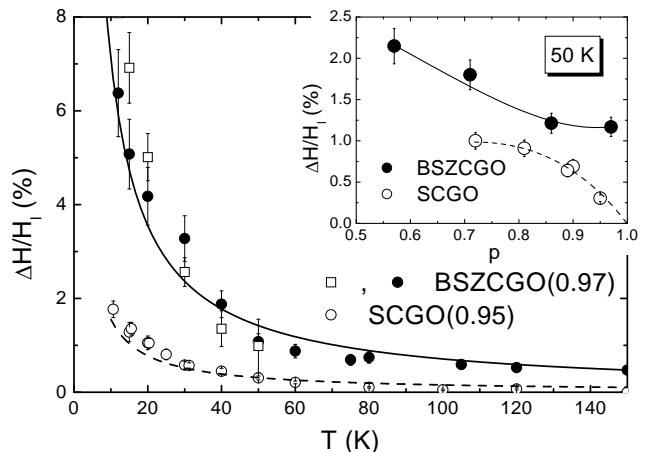
FIG. 14: Magnetic contribution to the NMR linewidth $\Delta H/H_l$. For BSZCGO(0.97), the data for the ^{71}Ga(2) ($\square$) are rescaled by a factor 6, corresponding to the ratio of the coupling constants, deduced from the high temperature shifts. $\bullet$ are for $\Delta H/H_l[^{71}$Ga(1)]. The lines are $\propto 1/T$ Curie-like fits. Inset: p-dependence of $\Delta H^{71}[^{71}$Ga(1)] at 50 K for SCGO(p) and BSZCGO(p). The lines are guides to the eye.

underlines the magnetic origin of the low-temperature broadening.

Figure 14 presents the linewidth obtained for SCGO(0.95) and for a comparable dilution in BSZCGO(0.97). Surprisingly, the Curie upturn in BSZCGO(0.97) is four times larger than in SCGO(0.95). This ratio cannot be explained by a higher hyperfine coupling constant for BSZCGO, since, as mentioned in Sec. II B, the constants C_{NMR} obtained from the high-temperature Curie-Weiss analysis of the shift in SCGO and BSZCGO point to the opposite variation. Further insight concerning this mismatch between the two HFMs can be gained by plotting the widths as a function of
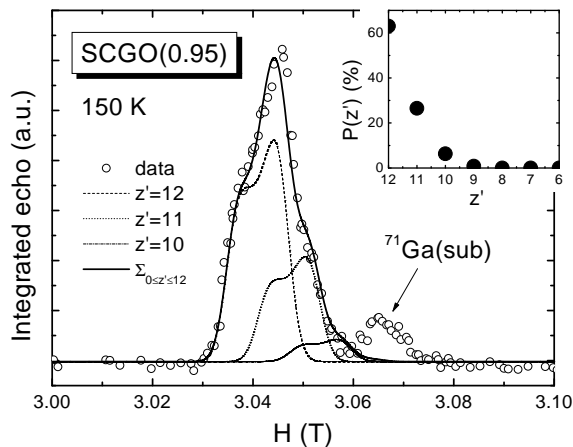
FIG. 15: ^{71}Ga(1) spectrum at 150 K in SCGO(0.95) ($\nu_l \approx$ 40 MHz). The lines are quadrupolar powder pattern simulations with the parameters of Tab. I, shifted with a value proportional to z', the number of NN Cr^{3+} for a site. Their area is weighted by the probability $P(z')$ when $p = 0.95$, presented in the inset.
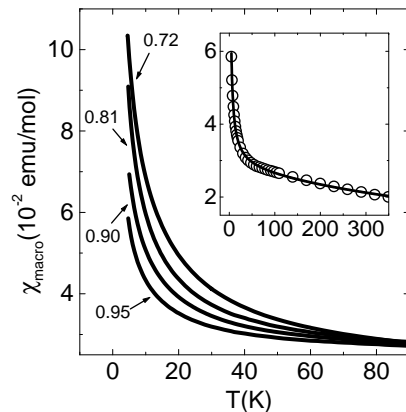

FIG. 16: Low-temperature macroscopic susceptibility (SQUID) for some SCGO Cr-concentrations. Inset: SCGO(0.95) data (open circles) fitted with Eq. 5.

dilution at a given temperature (inset of Fig. 14). In SCGO the width extrapolates to 0 when $p = 1$, which shows that the width is only related to dilution. On the contrary, in BSZCGO the width reaches an asymptotic non-zero value for $0.86 \leq p < 1$. As a first assumption, one could wonder whether the dilution of the lattice is larger than the nominal one. This can be ruled out since (i) the expected evolution of the line shape with p is found at 300 K (see the following) (ii) muon spin relaxation measurements indicate a regular evolution of the dynamical properties with p (Sec. III). Therefore, the increased low-temperature upturn in BSZCGO comes from dilution-independent paramagnetic defects, which are not present in SCGO.

We may already rule out possible scenarios which could be responsible for the low-temperature broadening. For instance, the broadening generated by the suppression of chromium ions in the nuclear environment. Such a distribution is present in the Ga(1) NMR spectra of SCGO and of BSZCGO, but is only responsible for a minor broadening of the line as shown in Fig. 15 for SCGO(0.95). This broadening mechanism results from the fact that each Ga(1) nucleus has a probability $P(z')$ (inset of Fig. 15) to have z' chromium neighbors ($0 \leq z' \leq 12$). Assuming that the Ga/Cr substitution does not affect the Ga-O-Cr hyperfine couplings and that all the chromium ions have the same susceptibility, the shift of a Ga(1) nucleus surrounded by z' neighboring chromium ions is then proportional to z', according to Eq. 1. To construct the spectrum, each gallium nucleus is associated to a quadrupole line simulated with the parameters of Tab. I, with a shift reflecting its Cr-environment and an intensity weighted by the total number of gallium nuclei having the same environment, i.e. weighted by $P(z')$. The simulated line perfectly matches the experimental

Ga(1) NMR line at 150 K (Fig. 15). However, the broadening resulting from this distribution scales with the susceptibility, hence with the shift K. Since K decreases at low temperature, this broadening mechanism cannot explain the low-temperature upturn of the width. For the same reason, a spatial distribution of the hyperfine constant, which yields also a width $\propto K$, cannot justify the broadening observed and also has to be ruled out [102]. Even if a such refined analysis is not possible in BSZCGO because of a stronger broadening than SCGO, similar conclusions are derived for this compound [56]. Hence, the explanation for the low-temperature broadening must be searched elsewhere (see Sec. II C 3).

2. SQUID

The SQUID measurements were carried out over a wide range of Cr-concentrations ($0.29 \leq p \leq 0.97$) for temperatures down to 1.8 K (no difference was observed between the Field Cooled and Zero Field Cooled susceptibility above the freezing temperature T_g in a field of 100 G). Figure 16 presents the typical low-temperature macroscopic susceptibility of these HFMs. Like the NMR linewidth, the susceptibility exhibits a low-temperature upturn, increasing with growing dilution. In Sec. II B, by a comparison between the NMR shift and the macroscopic susceptibility, we established that χ_{macro} must be a two-component susceptibility, and, in particular, that it should possess, compared to the shift, a paramagnetic susceptibility χ_{def} to explain its low-temperature upturn. The dilution-dependent upturn of χ_{macro} in Fig. 16 therefore establishes that χ_{def} is related to the Ga/Cr substitution in SCGO(p). However, we also know from NMR that there also extra paramagnetic contributions, related to intrinsic defects in BSZCGO for example.

In order to quantify the low-temperature dependence of the susceptibility, we follow Ref. 65 and fit χ_{macro} by
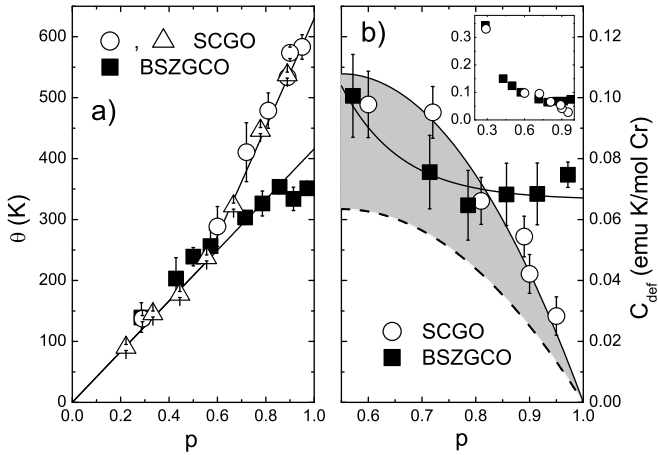
FIG. 17: Fits of the SQUID data (Eq. 5). a) △ come from Ref. 50. The lines are guide to the eye. b) The dashed line represents the Kagomé bilayers defects contribution to $C_{\text{def}}(p)$ in SCGO(p), the other lines are guide to the eye. The grey area represent the Cr(c) contribution in $C_{\text{def}}(p)$ for SCGO(p) (see text). Inset: same data as (a) for a broader range of p.

a two component expression:

$$\chi_{\text{macro}} = \frac{C}{T + \theta} + \frac{C_{\text{def}}}{T + \theta_{\text{def}}} \ . \qquad (5)$$

The first Curie-Weiss term roughly takes into account the contribution from the Kagomé bilayer and governs the behavior of χ_{macro} at high temperature. The second term, the more relevant for this section, also *a priori* Curie-Weiss, quantifies the contribution of χ_{def}. A more accurate fit of χ_{macro} would consist in using a low-temperature susceptibility mimicking the NMR shift. Such a fit, however, yields the same qualitative results as presented below.

From these fits (e.g. inset of Fig. 16), an effective moment per Cr^{3+} is extracted, $p_{eff} = 4.1 \pm 0.2/\mu_B$ in both SCGO [40] and BSZCGO, close to the $3.87/\mu_B$ expected for $S = \frac{3}{2}$ spins. In BSZCGO, the Curie-Weiss temperature is found to increase with p (Fig. 17a), in agreement with mean-field theory. From the linear variation, following the procedure described in Sec. II B, we extract $J = 40$ K [41], consistent with our NMR results. However, two linear regimes of $\theta(p)$ are observed for SCGO(p), below and above $p \sim 0.55$. This was first reported in Ref. 50 and cannot be understood in terms of simple mean field theory. Taking into account a third term in Eq. 5, corresponding to the susceptibility of the Cr(c) pairs in SCGO, derived in Ref. [40] and vanishingly small below 50 K, does not affect this result.

The second term in Eq. 5 is introduced to fit the low-temperature behavior of the defects. For all samples studied, it is close to a pure Curie law, within error bars. The values of the Curie constants C_{def} extracted are presented in Fig. 17b. A p-dependence qualitatively similar to the NMR width is found and C_{def} extrapolates again to 0 for $p = 1$ in SCGO, whereas it displays a finite value

in BSZCGO. When the Cr-concentration is $p \leq 0.8$, the dependency of C_{def} is qualitatively the same in both systems (inset of Fig. 17b). To give an order of magnitude, this term represents, for the purest samples, a number of $S = \frac{1}{2}$ paramagnetic spins equal to the number of spin vacancies in SCGO(p) [40] and to 15-20% of the number of Cr^{3+} spins in BSZCGO(p) [41].

3. Paramagnetic defects: discussion

The NMR and the macroscopic susceptibility measurements indicate that there are paramagnetic defects in SCGO and BSZCGO. Some of them are related to the spin vacancies in the Kagomé bilayers and affect the neighboring chromium ions in such a way that their overall behavior is paramagnetic. These defects therefore yield information on how the correlated spin network of the Kagomé bilayer responds to the presence of the vacancy. In the following, we discuss this point as well as the presence of other types of defects in both compounds.

The second type of defects result from lattice imperfections in BSZCGO, and from the dilution of the spin-pair sites in SCGO. Unfortunately, in the case of BSZCGO the second type of defect dominate the paramagnetic response, and in this compound, on the contrary of SCGO, a fine analysis of the spin-vacancy defects cannot be carried out, even by Ga(1) NMR.

a. Spin vacancies. In AFM systems such as the 1D spin chains [66, 67] the quasi-2D spin ladders [68] and the 2D cuprates [69] it is now well established that a vacancy (or a magnetic impurity) generates a long range oscillating magnetic perturbation and creates a paramagnetic-like, i.e. not necessarily $\propto 1/T$, component in the macroscopic susceptibility. The symmetric broadening of the NMR line observed in these systems is related to the oscillating character of the perturbation. The dilution effects of the Kagomé bilayer would then be described by the same physics of these correlated systems.

In SCGO, the symmetric feature of the Ga(1) NMR line indicates that spin vacancies induce a perturbation extended in space. This rules out descriptions of the defect in terms of uncorrelated paramagnetic centers [65, 70], since the broadening of the line would then be asymmetric. Hence, given the AFM interactions of the Kagomé bilayer, the perturbation was assigned to a staggered polarization of the network [40]. The exact diagonalization of 36 spin $\frac{1}{2}$ clusters on the Kagomé lattice with spin vacancies by Dommange *et al.* confirms this interpretation [23]. They show that within an RVB ground state, the spin-spin correlations around a vacancy are enhanced, and that the magnetization is staggered around it, a picture that should also hold for higher spin values. However, it seems that the image of a simple envelope of the staggered magnetization, like the Lorentzian now granted in High T_c cuprates [69], is not correct here since this localization of singlets around the vacancies shifts the staggered cloud from the non-magnetic impurity. Al-

though the agreement is qualitative at the moment, further work is required within this framework for a quantitative modelling of the NMR lineshape.

b. Bond disorder in BSZCGO. We previously saw that in BSZCGO(p), low temperature macroscopic susceptibility and NMR width data can be both satisfactorily accounted for, only if a novel p-independent defect-like contribution is taken into consideration, a result somehow surprising in view of the close similarity between the Kagomé bilayers of SCGO and BZSCCGO. The only major change lies in the 1:1 random occupancy of the Ga(1) site by Ga^{3+} or Zn^{2+} ions which induces different electrostatic interactions with the neighboring ions. As an example, distances to O^{2-} in a tetrahedral environment vary from $r_{Ga^{3+}-O^{2-}} = 0.47$ Å to $r_{Zn^{2+}-O^{2-}} = 0.60$ Å which is at the origin of a change of the average Ga(1)-O bonds, from 1.871 Å for SCGO [42] to 1.925 Å in BSZCGO [37]. Similarly, one expects that the Cr^{3+} will be less repelled by Zn^{2+} than by Ga^{3+}, which certainly induces magnetic bond-disorder, i.e. a modulation of exchange interactions J between neighboring Cr^{3+}. From Eq. 4, one can estimate that a modulation as low as 0.01 Å in the Cr^{3+}-Cr^{3+} distances would yield a 10% modulation of J.

The presence of non-perfect equilateral triangles classically induces a paramagnetic component in the susceptibility of the frustrated units [70]. The fact that we do not observe any extra Curie variation as compared to SCGO(p) in the average susceptibility, probed through the NMR shift K (Fig. 12), indicates that such unbalanced exchange interactions only induce a staggered response in the same manner as spin vacancies. Whether this could be connected with the localization of singlets in the vicinity of defects and a staggered cloud around them, like for spin vacancies, should be more deeply explored. This might highlight the relevance of a RVB approach to the physics of the Kagomé network. Further insight into the exact nature of the defects likely requires a better determination of the bond disorder through structural studies at low T, to avoid the usual thermal fluctuations at room T.

c. Broken spin-pairs in SCGO. The Ga/Cr substitution on a Cr(c) site of SCGO could in principle break a Cr(c)-Cr(c) spin pair and free a paramagnetic spin, which then could contribute to the paramagnetic upturn of χ_{macro}. However, this contribution turns out to be small. That the broken spin-pair susceptibility is negligible, can be deduced by comparing NMR and SQUID measurements for SCGO and BSZCGO. The starting point is to notice that the crossing between the variation of the curie constants C_{def} of both samples determined by the fits of Eq. 5 to the macroscopic susceptibility (Fig. 17b), is not observed in the NMR width (inset of Fig. 14). Considering from our NMR analysis that there is a 20% difference between the hyperfine coupling, we can evaluate that the scaling factor between $\Delta H/H_l(p)$ and $C_{def}(p)$ should be 20% larger in BSZCGO(p) than in SCGO(p). An error bar of 10% comes from the pos-

sible difference between the bilayer susceptibility measured with NMR and SQUID, since the Ga(1) nuclei do not probe stoichiometrically the magnetic sites Cr(b) and Cr(a) [103]. We first determine the scaling factor $[\Delta H/H_l(p)]/C_{def}(p)$ in BSZCGO(p), where 100% of the magnetic ions belong to the Kagomé bilayers. With the same ratio, the $\Delta H/H_l(p)$ data for SCGO(p) yield therefore a lower $C_{def}(p)$ than the measured one, out of the error bars [dashed line in Fig. 17b]. This difference is likely due to the Cr(c) pairs dilution in SCGO(p). Their contribution which, is not probed with the Ga(1) NMR [grey area in Fig. 17b], corresponds to a $0.04p$ Cr^{3+} $S = \frac{3}{2}$ paramagnetic term, whereas a $2p/9$ proportion would be expected in the case of a stoichiometrically substituted sample. This substoichiometric contribution of the Cr(c) site is consistent with neutron diffraction measurements [40].

III. SPIN DYNAMICS AND MAGNETIC EXCITATIONS

A. Muon: an appropriate probe of dynamics

We mentioned that an abrupt loss of the Ga(1)-NMR intensity occurs below 10 K (Fig 10). Hence, Ga(1)-NMR cannot be employed to probe the low-temperature magnetic properties of SCGO and of BSZCGO. This is unfortunate, since the low-temperature spin dynamics reseal, in particular, clue information concerning the ground state of these systems. On the contrary, due to the smaller coupling of the muon to the electronic moments and a shorter time window than the NMR one, the Muon Spin Relaxation (μSR) technique has proven to be a front tool for the study of quantum dynamical states in a vast family of fluctuating systems.

The electronic dynamics is commonly probed, either for NMR or for μSR, through the measurements of the longitudinal relaxation time, necessary to recover the thermodynamic equilibrium after the excitation of the nuclear spin or the muon spin systems. However, while the out-of-equilibrium state is reached using *rf* pulses in NMR, the muon spin system is already in an excited state. Indeed, muons (μ^+, $S = \frac{1}{2}$) are implanted in the sample, 100% spin polarized along the z axis. Therefore, the muon spins always depolarize to reach the Boltzmann distribution and μSR can be performed in zero external field, contrary to conventional NMR [71]. The time dependence of their *polarization* $P_z(t)$ along the z axis is studied through their decay into a positron [72] and is directly linked to both the spin fluctuations (the time correlation function of the local field H_μ is usually exponential, i.e., $\langle \mathbf{H}_\mu(0) \cdot \mathbf{H}_\mu(t) \rangle / \langle H_\mu(0)^2 \rangle = \exp(-\nu t)$) and the (random) local field distribution, characterized by a width Δ/γ_μ (γ_μ is the muon gyromagnetic ratio). The longitudinal relaxation times is related to the spin-correlation function through $1/T_1 \sim \int_0^\infty \langle \mathbf{S}(0) \cdot \mathbf{S}(t) \rangle \cos(\gamma_\mu H_{LF} t) dt$. Zero field and longitudinal field (LF) μSR experiments,

where the external field H_{LF} is applied along the z axis, allow for instance to distinguish magnetic (randomly or ordered) frozen states from dynamical ones [73, 74]. Moreover, whereas specific heat is sensitive to all kinds of excitations, including low-lying singlets at low temperature in the Kagomé bilayer samples [46], the muons probe *magnetic* excitations *only*, with a specific range of frequencies ($\sim 10^9$ Hz) sitting in a typical time window (10 ns-10 μs) in between NMR and neutron experiments.

We present here our μSR study of the spin dynamics in SCGO(p) and BSZCGO(p) [56, 58]. We first show that while conventional μSR polarization functions can be used in the whole temperature range for the very diluted samples and in the high temperature regime ($T \gtrsim 3T_g$) for the purest ones, they cannot be used satisfactorily in the low temperature regime in the latter case ($p \gtrsim 0.7$). Moreover, in this first step, we qualitatively show that the magnetic state of all the samples is dynamical down to the experimental limit of 30 mK (Sec. III B). We further use a model independent analysis of the data, simply taking the time necessary for the muon spin polarization to decrease down to the value $1/e$. The comparison between SCGO and BSZCGO clearly shows a correlation between the muon spin relaxation rate and T_g, suggesting that this freezing temperature is not an impurity phase. On the contrary, it seems to be closely linked to the slowing down of the spin dynamics in the bulk sample (Sec. III C). Finally, a phenomenological model for the muon relaxation, based on sporadic dynamics due to spin excitations in a singlet sea, proposed by Uemura *et al.* [49], is extended to all fields- and temperature- range. Its connection to the RVB picture is discussed, and we argue that such coherent states might mediate the interactions between impurities, which induce the spin glass freezing (Sec. III D).

B. Conventional approaches

1. High-temperature behavior

At high temperature, a conventional paramagnetic behavior is found for all the samples, with a stretched exponential variation of $P_z(t) = \exp[-(\lambda t)^\beta]$. Figure 18 shows that as expected, $\beta \to 1$ in the dense magnetic cases [73] (in our case with a high coverage of the Kagomé bilayer lattice with Cr^{3+}) and $\beta \to 0.5$ in the dilute cases [74] (i.e. with a low coverage).

We can give here an estimate of the fluctuation frequency in this temperature range and of the NMR time window which would be required to measure this spin dynamics. At ~ 50 K, the muon relaxation rate is $\lambda \sim 0.03$ μs^{-1} and 0.01 μs^{-1} in SCGO(0.95) and BSZCGO(0.97). In this appropriate fast fluctuating paramagnetic limit, the fluctuation rate can be estimated from $\nu \sim \sqrt{z}JS/k_B\hbar \sim 2 \times 10^{13}$ s^{-1} [49] using the coupling $J \approx 40$ K determined previously by NMR, and the average number $z = 5.14$ of Cr nearest neighbors. We ex-
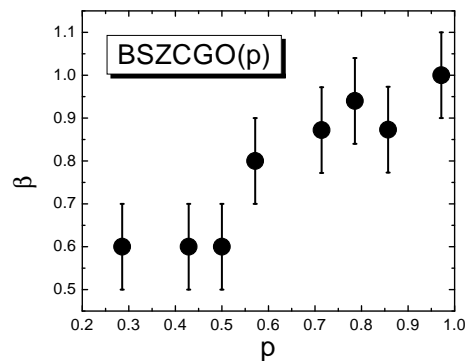

FIG. 18: Exponent $\beta(p)$ in BSZCGO(p) using the relaxation function $P_z(t) = exp[-(\lambda t)^\beta]$ appropriate for the fast fluctuations limit at high temperature ($T \geq 10$ K.).
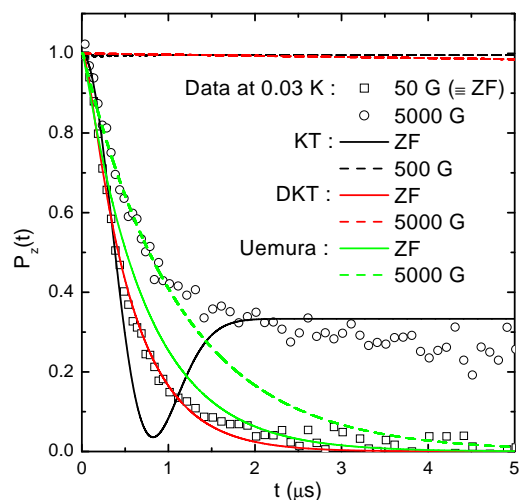

FIG. 19: BSZCGO(0.97) data at 0.03 K. The lines are fits with different models (see text). We used $\Delta \approx 2$ μs^{-1}, 4 μs^{-1} ($\nu \approx 17$ μs^{-1}) and 65 μs^{-1} ($\nu \approx 600$ μs^{-1})for the static, dynamic and "Uemura" cases respectively.

tract $\Delta = \sqrt{\lambda\nu/2} \sim 600$ μs^{-1} and 300 μs^{-1}, which corresponds to an average field at the muon sites of 7000 G and 3500 G for SCGO and BSZSCGO respectively.

Since the relationship between the longitudinal relaxation time T_1 measured in NMR and μSR is $T_1^{NMR}/T_1^{\mu SR} \sim [\Delta/(^{71}\gamma^{71}A)]^2$, where $^{71}A \sim 70$ kOe/μ_B is the hyperfine coupling constant of the ^{71}Ga nuclei obtained from NMR experiments, we can estimate that $T_1^{NMR}/T_1^{\mu SR} \sim 5$. This is consistent with our data $[T_1^{NMR} \sim 100$ μs at high temperature and establishes that below 5 K, the relaxation must be $T_1^{NMR} \sim 1$ μs, which is non-measurable as it lies out of the NMR time window. Such a small relaxation time is responsible for the wipeout of the Ga-NMR intensity (Fig. 10).

2. Failure of conventional approaches at low temperature for the purest samples

The derivation of zero field and longitudinal field μSR relaxation functions is presented in Ref. 73, 74 for textbook cases. We first rule out the possibility of some static freezing as the source of the muon relaxation. Two options can be considered. (i) In *randomly* frozen (static) magnetic states, the major results are the following: first, the muon spin polarization displays a "$\frac{1}{3}$ tail" in zero external field, i.e, $P_z(t \geq 5/\Delta) \to \frac{1}{3}$. Indeed, $\frac{1}{3}$ of the frozen magnetic internal fields are statistically parallel to z and do not contribute to the muon spin depolarization. Second, $P_z(t)$ is "decoupled", i.e., does not relax, for longitudinal fields $H_{LF} \gtrsim 10\Delta/\gamma_\mu$. (ii) In the case of *ordered* magnetic states and powder samples, the "$\frac{1}{3}$ tail" is still observed in zero field experiments for the same reasons, but oscillations appear in $P_z(t)$, which correspond to well defined local fields.

One should notice that nuclear moments which appear static on the μSR time window always contribute to the time-evolution of the polarization. A small longitudinal field of the order of a few 10 G ($\Delta_{ND} \sim 0.1~\mu s^{-1}$) is commonly applied to "decouple" this contribution. In other words, since the electronic and dipolar contributions are multiplied, such a contribution, if any, "disappears" and only the electronic contribution, not perturbed by such low fields, is measured. Hence, experiments performed in $H_{LF} \sim 100$ G are equivalent to a zero field measurement without nuclear dipoles.

Figure 19 shows $P_z(t)$ measured in BSZCGO(0.97) at 0.03 K for $H_{LF} = 50$ G and for $H_{LF} = 5000$ G. Neither oscillations nor a $\frac{1}{3}$ tail are observed when $H_{LF} = 50$ G. Although not emphasized in the figure, one can note that the initial polarization is Gaussian, which is even clearer in SCGO(p) [49]. In a *static* case, such a shape is observed in dense magnetic randomly frozen systems, where the polarization is given by the Gaussian Kubo-Toyabe (KT) function [73]. We fitted our data at short times with this function in zero field, and plot the expected polarization when $H_{LF} = 500$ G in Fig. 19, which is found to be completely decoupled. This contrasts with our experimental finding, i.e., the polarization at 5000 G is hardly decoupled. *The lack of the $\frac{1}{3}$ tail, the absence of oscillations and of decoupling effect show that the magnetic state of BSZCGO(0.97) is fluctuating at 0.03 K.* All these considerations remain valid in both SCGO(p) and BSZCGO(p) compounds when $p \gtrsim 0.6$.

The computation of the *dynamical* relaxation functions is based on a strong collision approximation [73]. Using the corresponding Dynamical Kubo-Toyabe (DKT) function, analytically derived by Keren when $\nu \geq \Delta$ [75], allows us to fit the zero field data on the whole time range (Fig. 19). Again, the experimental data is much less sensitive to the applied field $H_{LF} = 5000$ G than the expected polarization.

This so called "undecouplable Gaussian line shape" was first reported in Ref. 49 for SCGO(0.89) and

further in other Kagomé compounds [57, 76, 77] or spin singlet compounds like the doped Haldane chain $Y_{2-x}Ca_xBaNiO_5$ [78]. Uemura *et al.* proposed a relaxation model [49], presented further in this paper, which catches some of the facets of this relaxation. For now, we just notice that this model cannot justify our data for all fields (Fig. 19), even if it shows a lower decoupling effect, consistent with our (and previous) observations. Before going further with more complex models (Sec. III D), we will first, in the following, give qualitative arguments to characterize the low temperature magnetism of our samples.

In order to illustrate the evolution of the properties with p, we present two typical low and high occupations p of the Kagomé bilayers in Fig. 20 which emphasize the qualitative differences for various frustrated network coverage rates p. In addition to the high temperature behavior already commented, the evolution of $P_z(t)$ at low temperature is markedly different. For $p = 0.97$, the relaxation rate increases by more than two orders of magnitude to reach a temperature-independent value for $T \lesssim T_g \approx 1.5$ K [Fig. 20(b)], with the undecouplable character presented above. For a low coverage rate, $p = 0.43$, we also find a dynamical state but, at variance with the previous case, only a weak temperature-dependence is observed. Also, the polarization displays a square root exponential decay for *all* temperatures [Fig. 20(a)] and for any longitudinal field H_{LF} [Fig. 20(c)]. A weak plateau of the relaxation rate is still observed below 0.5 K but is no more present for $p = 0.3$, where $P_z(t)$ is found weakly temperature- and H_{LF}-dependent. This is typical of the pure paramagnetic fast fluctuations limit for dilute magnetic systems, which contrasts with the results of SQUID measurements showing that strongly frustrated antiferromagnetic interactions are still present. This is the so called "cooperative paramagnetism".

C. Model independent basic analysis

As a first step to a quantitative analysis, we estimate the muon spin relaxation rate λ using the $\frac{1}{e}$ point of the polarization $P_z(t)$, as discussed in Ref. 57. This allows to single out information about two important issues using a simple model-independent analysis: the role of the spin glass-like transition and the impact of the spin vacancies on the dynamics.

From high temperature, λ increases by more than two orders of magnitude down to T_g for both kagome bilayers at their highest level of purity, to reach a relaxation rate plateau $\lambda_{T\to 0}$ for $T \lesssim T_g$ [49, 57]. Using a temperature-scale twice larger for SCGO(0.95) than in BSZCGO(0.97), the temperature dependence of λ of both samples perfectly scales on the temperature axis as shown in Fig. 21 [104]. This ratio is very close to the 2.3(2) ratio between their freezing temperatures T_g, which points to a link between the formation of the spin glass-like state
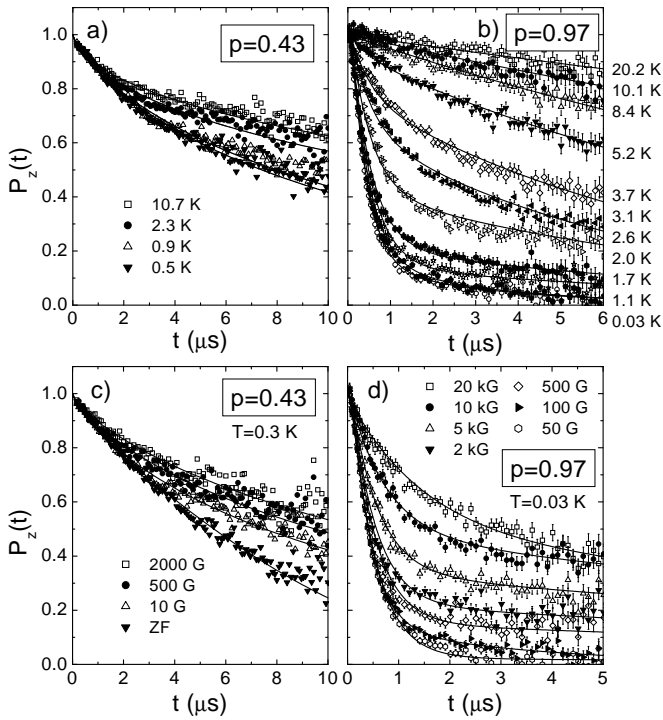
FIG. 20: a,b) temperature-dependence of the muon polarization $P_z(t)$ in BSZCGO under weak H_{LF} (10 G for $p = 0.43$ and 100 G for $p = 0.97$). Notice the different time scales for both samples. c,d) H_{LF}-dependence at base-temperature. The line for $p = 0.43$, ZF, is a square-root exponential times the Kubo-Toyabe function in zero field ($\Delta_{ND} \sim 0.08$ μs^{-1}), accounting for the nuclear dipole contribution. The other lines are fits described in the text.

and the presence of fluctuations. This seems to be a quite common feature of various systems with a singlet ground state [49, 57, 76, 77, 78].

In Fig. 22 we report the variation of $\lambda_{T \to 0}(T)$ for various BSZCGO(p) samples and compare them to SCGO(p) [49, 57]. Although additional p-independent defects are dominant in BSZCGO(p), as evidenced by SQUID and NMR measurements, it is very surprising to find, for the two systems, a very similar quantitative low-temperature relaxation rate $\lambda_{T \to 0}$ with increasing Cr-concentration over the *entire* p-range studied. Therefore we conclude that *only* defects related to *dilution* of the frustrated magnetic network influence the relaxation rate.

In a classical framework, a coplanar arrangement with zero-energy excitation modes, involving spins on hexagons, was proposed in the literature to be selected at low temperature [79]. Inelastic neutron scattering experiments on SCGO and the spinel compound $ZnCr_2O_4$ are indications in favor of such excitations [33, 48]. Therefore, one expects the muon spin relaxation to scale with the number of fully occupied hexagons, $\propto p^6$. In Fig. 22, the BSZCGO(p) data altogether with our SCGO($p \geq 0.89$) samples indicate that $\lambda_{T \to 0}(p)$ is well accounted for by adding a dominant p^6 term to the p^3 term proposed

for SCGO($p \leq 0.89$) in Ref. 57. In a case of purely dipolar couplings of the muon with the electronic magnetic moments, the average of the local dipolar field is given by $\Delta \propto \langle \sum_i 1/r_i^3 \rangle \propto p$, where the sum is made over the Cr^{3+} ions, r_i is the distance between the muon and the ith position and $\langle \cdot \rangle$ is the average over the muon positions. One therefore obtains $\lambda(p) \sim \Delta(p) \propto p$ in the case of slow fluctuations and $\lambda(p) \sim 2\Delta(p)^2\nu/(\nu^2 + \gamma_\mu^2 H_{LF}^2) \propto p^2$ in the case of fast fluctuations, i.e., $\lambda(p) \propto p^\eta$, with $\eta \leq 2$, which is not consistent with our data. This indicates that the relaxation is not induced by single spin excitations but rather *collective* excitation processes extending at least on triangles and/or hexagons. However these excitations still involve only a finite number of spins since the increase of spin vacancies only affect smoothly the
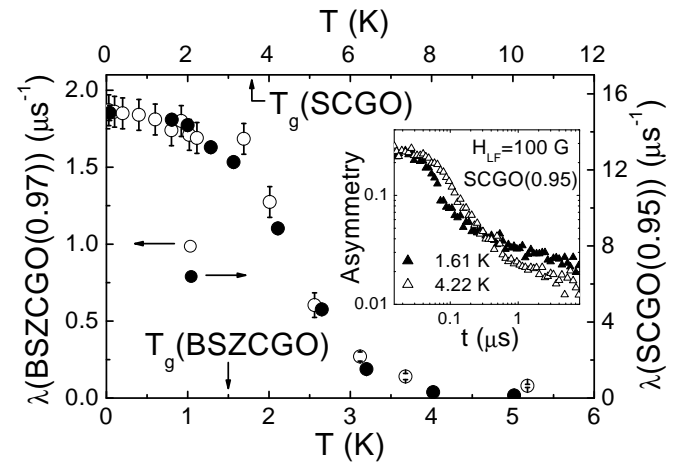

FIG. 21: Comparison of the evolution of the muon spin relaxation rate λ vs. T in BSZCGO(0.97) and SCGO(0.95), from a $1/e$ analysis. Inset: recovery of a part of the asymmetry at low temperature and long times in SCGO(0.95) below T_g (log-log scale).
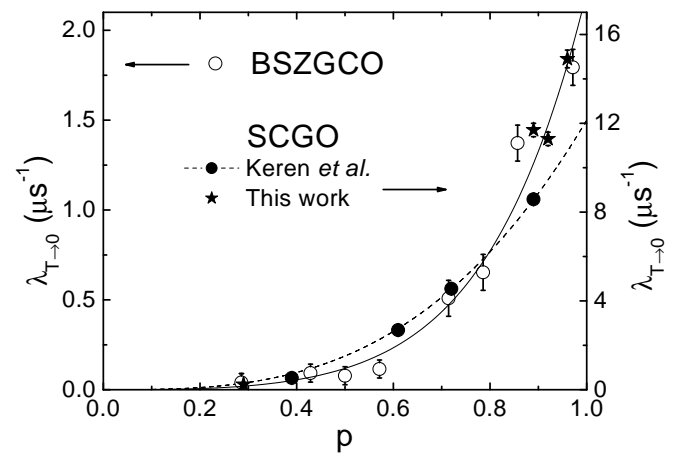

FIG. 22: p-dependence of $\lambda_{T \to 0}$ for BSZCGO(p) (open symbols) and SCGO(p) (full symbols). Continuous (dashed) lines are $\sim p^3 + 1.9(3)p^6$ ($\propto p^3$, [57]) fits.
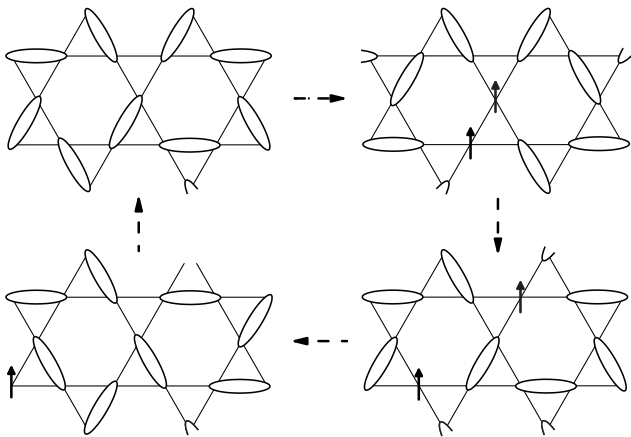
FIG. 23: Schematic representation of the creation and deconfinement of a spinon in a RVB ground state on a Kagomé lattice.

spin dynamics. On the contrary, a more pronounced effect is observed in the $S = \frac{1}{2}$ Kagomé-like compound volborthite [77].

D. RVB ground state with coherent unconfined spinons

Finding a phenomenological model reproducing the polarization $P_z(t)$ for *all* fields, *all* temperatures and *all* dilutions has been for long a pending challenge in the analysis of these μSR experiments in Kagomé frustrated antiferromagnets. In the quantum framework of a singlet ground state, one needs unpaired spins, i.e. isolated magnetic moments, in order to generate magnetic excitations responsible for the muon spin relaxation. Such excitations can be ascribed to unconfined spinons [19], for which the location of spin $\frac{1}{2}$ varies in time with no loss of coherence of the excited state (Fig. 23). Hence, a given muon spin couples to a spin only a short fraction ft of the time t after implantation and one can use a model of "sporadic" field fluctuations to describe $P_z(t)$.

This was the initial guess by Uemura *et al.* to account for the weakness of the field dependence of $P_z(t)$ at low temperature in SCGO(0.89) [49], although the spins are $S = \frac{3}{2}$. In the absence of any theoretical predictions, we will just assume that the mechanism is comparable. This polarization is given by a "sporadic" dynamical Kubo-Toyabe function, $P_z^K(ft, \Delta, H_{LF}, \nu)$, which rewrites simply $P_z^K(t, f\Delta, fH_{LF}, f\nu)$. Δ/γ_μ is the local field created on the muon site by a paramagnetic neighboring released spin with a fluctuation frequency ν and a corresponding exponential time correlation function $\exp(-\nu t)$. Δ is therefore related to the muon location in the unit cell and its average is assumed to be p-independent for a given system but is expected to vary from BSZCGO to SCGO. The Gaussian at early times, the weakness of the field dependence and a dynamical relaxation down

to 0 are altogether related to the f factor and $\nu \sim \Delta$. In addition to this sporadic relaxation, we found that a more conventional Markovian relaxation needs to be introduced to fit the long times tail ($t \gtrsim 3 \mu$s) for all fields and temperatures. We therefore write

$$P_z(t) = x P_z^K(t, f\Delta, fH_{LF}, f\nu) + (1-x)e^{-\lambda' t}, \quad (6)$$

where x represents the weight of the short time sporadic dynamical function, associated with the spinons dynamics. In the following, we first detail how all these parameters can be reliably deduced from the data and sketch a physical picture consistent with our results.

We first present our analysis for $T \ll T_g$ in BSZCGO(p). In order to limit the number of free parameters, we make the minimal assumption that the external field does not influence the dynamics of the coherent spinon term. The dynamics (ν) and the average dipolar field created by a spinon on a muon site (Δ) are shared for all p and H_{LF}. For low fields, x is found close to 1 for the purest samples [Fig. 20(a,b)], making λ' a non-relevant fitting parameter. It also enables us to determine ν and Δ when $H_{LF} < 500$ G, for various p. The parameter f is adjusted for each p and its variation accounts for the evolution of $\lambda_{T\to0}(p)$. On the contrary, the high field data enable us to monitor the evolution of x with H_{LF} and to determine a value for λ'. We could not extend the fits below $p = 0.71$ since the weak field dependence prevents an unambiguous determination of the parameters.

We find perfect fits of our data [Fig. 20(d)] with $\nu \sim 1000 \mu$s^{-1}, $\Delta \sim 350 \mu$s$^{-1} \sim \gamma_\mu \times 4$ kG and an average value of $f \sim 0.006$. We find a nearly flat p-independent long time relaxation rate for $T \ll T_g$ [$\lambda' \sim 0.05 \mu$s^{-1}, ★ in Fig. 24(d)]. An important finding is that x is of the order of p at low fields [Fig. 24(a,b)]. This may be related to the theoretical computations showing that the correlations are enhanced around spin vacancies in the Kagomé lattice [23], which would destroy locally the spin liquid state. Besides, x decreases appreciably for $H_{LF} \sim 10$ kG whatever the value of p. We can associate this decrease to the existence of an energy scale ~ 1 K, which is of the order of T_g. Finally, we observe a linear variation of f with p [Fig. 24(c)] and f tends to vanish around $p \sim 0.5$, a limit consistent with our classical approach (Fig. 22). Indeed, since we find $\nu \sim \Delta$ when $T \to 0$, the relationship $f(p)\Delta \sim \lambda_{T\to0}(p)$ is expected. This indicates that even far from the substituted sites, the coherent state is somehow affected, e.g the density of spinons could be smaller.

As suggested by the similar p-variation of $\lambda_{T\to0}$ in both BSZCGO(p) and SCGO(p), we assume that the excitation modes are identical in both systems, i.e., f and ν are kept the same for comparable p. We find $\Delta \sim 1200 \mu$s^{-1} for our SCGO($p \geq 0.89$) samples, in agreement with previous work on SCGO(0.89) [49]. It is quite rewarding to find that a *common* physical picture underlies all the sets of data at low temperature for *both* Kagomé bilayers.

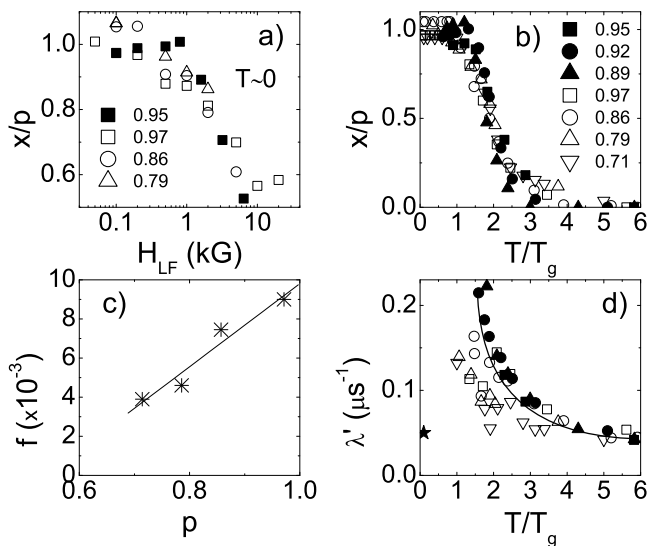We now extend the fits of the muon spin polarization

FIG. 24: Fitting parameters of Eq. 6 for BSZCGO and SCGO (open and full symbols). f is common for both systems.

$P_z(t)$ to the whole temperature-range [Fig. 20(b)], fixing f to its low-temperature value in order to limit the number of free parameters. It would also, phenomenologically, mean that once a spinon is created, its deconfinement process remains temperature independent, which is a quite reasonable assumption from a quantum point of view. As expected from the change of shape around T_g [49, 57], the weight x of the sporadic term decreases to finally enter a high-temperature regime [Fig. 24(b)] with an exponential muon relaxation ($x \rightarrow 0$). The similarity between the field- and temperature-dependence of x indicates that the sporadic regime is destroyed with an energy of the order of the freezing temperature T_g. Figure 22(b) displays a sharp crossover from one state to the other, between T_g and $3T_g$, corresponding to the λ steep decrease (Fig. 21), for both BSZCGO(p) and SCGO(p). For $T > T_g$, ν and λ' [Fig. 24(d)] decrease by one order of magnitude up to $10T_g$.

At high temperature, it is natural to think in terms of paramagnetic fluctuating spins. At lower temperatures, λ' seems to diverge at T_g and below, the weight of the exponential term at low fields ($1 - x \sim 1 - p$) could correspond to localized frozen spins, reflecting the glassy component measured by SQUID. It is noteworthy that T_g does not increase with $1 - p$ but rather decreases, at the opposite of the case of canonical spin glasses. We could further confirm the existence of such a frozen component in SCGO($p = 0.95$-0.89), since a clear recovery of a small part ($\sim 4\%$) of the asymmetry is found at long times [e.g. Fig. 21(inset)]. It is observed for $t \sim 100\,\lambda^{-1}$, which is out of the experimental range for BSZCGO(p).

To summarize, the picture based on a coherent RVB state, which magnetic excitations are mobile fluctuating spins $\frac{1}{2}$ on the Kagomé lattice, explains well the data, provided that (i) these excitations can be generated even

for $T \rightarrow 0$. This underlines the smallness of the "magnetic" gap, if any, typically $\Delta < J/1000$; (ii) an energy scale related to T_g (fields of the order of 10 kG or, equivalently, temperatures of the order of T_g, which vary very little with p) are high enough to destroy the coherent RVB type state ; (iii) the substitution defects are accounted for by an additional classical relaxation process.

E. Spin-Glass-like transition

The "intrinsic" spin-glass-like transition at T_g is one of the most puzzling observation in these frustrated magnets. Indeed, the origin of such a spin glass state in a disorder-free system still awaits for a complete understanding, although recent theoretical approaches catch some of the facets of this original ground state [80]. The most realistic model, presented by Ferrero et al. in Ref. 81, uses the so called "dimerized approach [14, 16], i.e., considers a geometry of the Kagomé lattice with two different kinds of equilateral triangles, corresponding to the Cr(b) layers in SCGO(p) and BSZCGO(p) (Fig. 3). It predicts a spin glass-like transition in the $S = \frac{1}{2}$ Kagomé lattice, related to the freezing of the chirality, with $T_g \sim 0.5J'$. Here, J' is the largest coupling in the Kagomé planes (corresponding to the thick lines in Fig. 3). Although $0.05J'$ is of the order of magnitude of the experimental T_g, the very similar values of the Cr-Cr bonds in both systems and Eq. 4 do not allow to predict a factor 2 in T_g.

From our μSR results, we propose an other interpretation which still awaits for theoretical confirmation. We find no energy gap for the spin $\frac{1}{2}$ excitations. This could explain quite well why the transition to the spin glass state is fairly independent of p. Indeed, in this framework, spinons could mediate the interactions between magnetic defects localized around spin vacancies. This is corroborated by all the scaling properties in T/T_g. The transition to the spin glass state would correspond then to the formation of the coherent singlet state rather than any interaction strength between defects. The bond defects inherent to BSZCGO(p) probably decrease the value of this coherent state energy scale since it is more favorable to create localized singlets in this geometry. This is qualitatively consistent with the twice lower spin glass transition temperature in this family.

F. Extension to other compounds?

We already noticed that the μSR undecouplable Gaussian line shape, altogether with a plateau of the relaxation rate, have been reported in other compounds, and now elaborate about the possible links between these systems.

The other Kagomé compounds, volborthite [77, 82, 83] and Cr jarosite [76] display the same properties as the

Kagomé bilayers and our phenomenological model seems correct.

Kojima *et al.* already noticed the similarity between SCGO and the doped Haldane chain $Y_{2-x}Ca_xBaNiO_5$ and SCGO(0.89) [78, 84]. However, contrary to the Kagomé bilayers, the relaxation function becomes more "conventional" when the system becomes purer, i.e., the muon spin relaxation function is a square root exponential in the pure system at low temperature. It is not surprising since in the pure Haldane chain one expects a Valence Bond Crystal [19]. Therefore no magnetic excitation are allowed at low temperature and no depolarization is expected in μSR. However, mobile excitations are added when the chains are doped [85], i.e. the muon spin relaxation becomes unconventional. This corresponds to the data and is consistent with our unconfined spinon phenomenological model.

Finally, Fukaya *et al.* reported the same behavior in $Sr(Cu_{1-x}Zn_x)_2(BO_3)_2$ for $x = 0$ and 0.02 [86]. This system displays, theoretically and experimentally, an exact singlet dimer state and its intrinsic susceptibility vanishes for $T \lesssim 3$ K [87, 88]. Nonetheless, a CW term, corresponding to 0.72% of $S = \frac{1}{2}$ impurities with respect to the Cu sites, is observed below 4 K [87], which is finally comparable, from the macroscopic susceptibility aspect, to the former cases of pure volborthite and pure $Y_2CaBaNiO_5$. However, according to us, there is today no clue about the possibility of mobile excitations in this magnetic network with a few percent of defects.

We conclude that *all* these systems display (i) a theoretical and/or experimental singlet ground state; (ii) a defect term observed through a low-temperature CW like upturn in the macroscopic susceptibility; (iii) a spin glass-like transition of this defect term at a temperature T_g (but $Sr(Cu_{1-x}Zn_x)_2(BO_3)_2$) [105]; (iv) a plateau of the muon spin relaxation rate below T_g.

It is important to notice that the clear experimental correlation between the muon spin relaxation rate plateau and the spin glass-like transition is strongly against a pure muon-induced effect argument for this plateau. Even if the muon has indeed an effect on the physics of these compounds, the λ plateau below T_g shows that a bulk transition occurs at this temperature, i.e. that this freezing cannot be due to isolated impurities.

Theoretical approaches are now required to link a possible unconfined spinons state to a spin-glass-like behavior and a relaxation plateau of the implanted muon spins. They could therefore corroborate our phenomenological approach.

IV. CONCLUSION

With Heisenberg spins and nearest neighbor couplings of the order of 40 K, the Kagomé bilayers of SCGO and BSZCCGO are today the archetypes of Highly Frustrated Magnets. The comparison between SQUID and NMR ex-

periments on the two slightly different compounds SCGO and BSZCGO allows us to isolate the intrinsic properties of the frustrated Kagomé bilayer geometry and to understand better the role of the (non)magnetic defects. We find that *defects* localized in the frustrated network induce a spatially extended response of the magnetic system, consistent with theoretical predictions. This response generates a Curie-like upturn in the macroscopic susceptibility at low temperature. However, local measurements of the susceptibility, using Ga NMR, show that the *intrinsic* susceptibility of the Kagomé bilayers decreases below 45 K, a temperature of the order of J. This behavior was also predicted theoretically and is consistent with short-ranged spin-spin correlations, on the order of the lattice parameter. We cannot give a definitive conclusion about the existence of a spin gap with NMR experiments because the gallium nuclei cannot be probed by NMR at low temperature. However a maximum value of $\sim J/10$ is found for such a gap.

We measured the spin dynamics using Muon Spin Relaxation experiments, down to 30 mK. We find that both systems SCGO and BSZCGO display a dynamical magnetic state down to this temperature, unconventional for the purest samples. Very simple considerations show that the spin-glass-like state, measured at $T_g \ll \theta_{CW}$ with macroscopic susceptibility techniques, is correlated to the slowing down of the Cr spin dynamics in the whole sample. The data are well accounted by a description based on unconfined spinons as the magnetic excitations and we suggest that this phenomenological approach remains valid for several spin singlet compounds at low temperature. Indeed, they all display striking similar aspects such as a spin glass transition of the magnetic defect channel in the macroscopic susceptibility and an undecouplable Gaussian line shape with a relaxation rate plateau of the muon polarization below this spin glass transition.

In all these systems the fast depolarization of the muon down to the experimental limit of $T \sim 30$ mK underlines the existence of magnetic excitations at low temperature and hence the weakness of an hypothetical unconfined spinon gap. An other spin dynamics study with Neutron Spin Echo technique is in progress and could give more details about this $T \to 0$ spin liquid state [89].

[1] P. W. Anderson, Mater. Res. Bull. **8**, 153 (1973).
[2] P. W. Anderson, Science **235**, 1196 (1987).
[3] G. Baskaran, Phys. Rev. Lett. **91**, 097003 (2003).
[4] B. Bernu, P. Lecheminant, C. Lhuillier, and L. Pierre, Phys. Rev. B **50**, 10048 (1994).
[5] A. P. Ramirez, in *Handbook on Magnetic Materials*, edited by K. J. H. Busch (Elsevier Science, Amsterdam, 2001), vol. 13, p. 423.
[6] R. Stewart, ed., *Proceedings of the Highly Frustrated Magnetism 2003 Conference, Grenoble, France* (2004), J. Phys.: Condens. Matter, **16**, S553-922.
[7] K. Binder and A. P. Young, Rev. Mod. Phys. **58**, 801 (1986).
[8] D. A. Huse and A. D. Rutenberg, Phys. Rev. B **45**, 7536 (1992).
[9] J. T. Chalker, P. C. W. Holdsworth, and E. F. Shender, Phys. Rev. Lett. **68**, 855 (1992).
[10] I. Ritchey, P. Chandra, and P. Coleman, Phys. Rev. B **47**, 15342 (1993).
[11] G. Misguich and C. Lhuillier, in *Frustrated Spin systems*, edited by H. T. Diep (World Scientific, Singapore, 2003), (cond-mat/0310405), and references therein.
[12] R. Moessner, Can. J. Phys. **79**, 1283 (2001).
[13] C. Zeng and V. Elser, Phys. Rev. B **51**, 8318 (1995).
[14] M. Mambrini and F. Mila, Eur. Phys. J. B **17**, 651 (2000).
[15] C. Waldtmann, H. U. Everts, B. Bernu, C. Lhuillier, P. Sindzingre, P. Lecheminant, and L. Pierre, Eur. Phys. J. B **2**, 501 (1998).
[16] F. Mila, Phys. Rev. Lett. **81**, 2356 (1998).
[17] G. Misguich, D. Serban, and V. Pasquier, Phys. Rev. B **67**, 214413 (2003).
[18] B. Canals and C. Lacroix, Phys. Rev. Lett. **80**, 2933 (1998).
[19] C. Lhuillier and P. Sindzingre, in *Quantum Properties of Low-Dimensional Antiferromagnets*, edited by Y. Ajiro and J. P. Boucher (Kyushu University Press, Fukuoka, 2001), p. 111, cond-mat/0212351.
[20] S. E. Palmer and J. T. Chalker, Phys. Rev. B **62**, 488 (2000).
[21] O. Tchernyshyov, R. Moessner, and S. L. Sondhi, Phys. Rev. Lett. **88**, 067203 (2002).
[22] M. Elhajal, B. Canals, and C. Lacroix, Phys. Rev. B **66**, 014422 (2002).
[23] S. Dommange, M. Mambrini, B. Normand, and F. Mila, Phys. Rev. B **68**, 224416 (2003).
[24] M. E. Zhitomirsky, A. Honecker, and O. A. Petrenko, Phys. Rev. Lett. **85**, 3269 (2000).
[25] J.-C. Domenge, P. Sindzingre, and C. Lhuillier, cond-mat/0502414.
[26] A. S. Wills, Can. J. Phys. **79**, 1501 (2001).
[27] Y. Narumi, K. Katsumata, Z. Honda, J. C. Domenge, P. Sindzingre, C. Lhuillier, Y. Shimoaka, T. C. Kobayashi, and K. Kindo, Europhys. Lett. **65**, 705 (2004).
[28] G. Lawes, M. Kenzelmann, N. Rogado, K. H. Kim, G. A. Jorge, R. J. Cava, A. Aharony, O. Entin-Wohlman, A. B. Harris, T. Yildirim, et al., Phys. Rev. Lett. **93**, 247201 (2004).
[29] N. P. Raju, M. Dion, M. J. P. Gingras, T. E. Mason, and J. E. Greedan, Phys. Rev. B **59**, 14489 (1999).
[30] A. Keren and J. Gardner, Phys. Rev. Lett. **17**, 177201 (2001).
[31] J. A. Hodges, P. Bonville, A. Forget, A. Yaouanc, P. Dalmas de Réotier, G. André, M. Rams, K. Królas, C. Ritter, P. C. M. Gubbens, et al., Phys. Rev. Lett. **88**, 077204 (2002).
[32] A. Keren, J. S. Gardner, G. Ehlers, A. Fukaya, E. Segal, and Y. J. Uemura, Phys. Rev. Lett. **92**, 107204 (2004).
[33] S. H. Lee, C. Broholm, W. Ratcliff, G. Gasparovic, Q. Huang, T. H. Kim, and S. W. Cheong, Nature **418**, 856 (2002).
[34] M. Harris, Nature **399**, 311 (1999).
[35] A. P. Ramirez, A. Hayashi, R. J. Cava, R. Siddhartan, and B. S. Shastry, Nature **399**, 333 (1999).
[36] X. Obradors, A. Labarta, A. Isalgué, J. Tejada, J. Rodriguez, and M. Pernet, Solid State Commun. **65**, 189 (1988).
[37] I. S. Hagemann, Q. Huang, X. P. A. Gao, A. P. Ramirez, and R. J. Cava, Phys. Rev. Lett. **86**, 894 (2001).
[38] A. P. Ramirez, G. P. Espinosa, and A. S. Cooper, Phys. Rev. B **45**, 2505 (1992).
[39] H. Ohta, M. Sumikawa, M. Motokawa, H. Kikuchi, and H. Nagasawa, J. Phys. Soc. Jpn. **65**, 848 (1996).
[40] L. Limot, P. Mendels, G. Collin, C. Mondelli, B. Ouladdiaf, H. Mutka, N. Blanchard, and M. Mekata, Phys. Rev. B **65**, 144447 (2002).
[41] D. Bono, P. Mendels, G. Collin, and N. Blanchard, Phys. Rev. Lett. **92**, 217202 (2004).
[42] S. H. Lee, C. Broholm, G. Aeppli, T. G. Perring, B. Hessen, and A. Taylor, Phys. Rev. Lett. **76**, 4424 (1996).
[43] L. J. de Jongh and A. R. Miedema, Adv. Phys. **50**, 947 (2001).
[44] A. P. Ramirez, G. P. Espinosa, and A. S. Cooper, Phys. Rev. Lett. **64**, 2070 (1990).
[45] P. Lecheminant, B. Bernu, C. Lhuillier, L. Pierre, and P. Sindzingre, Phys. Rev. B **56**, 2521 (1997).
[46] A. P. Ramirez, B. Hessen, and M. Winklemann, Phys. Rev. Lett. **84**, 2957 (2000).
[47] P. Sindzingre, G. Misguich, C. Lhuillier, B. Bernu, L. Pierre, C. Waldtmann, and H. U. Everts, Phys. Rev. Lett. **84**, 2953 (2000).
[48] C. Broholm, G. Aeppli, G. P. Espinosa, and A. S. Cooper, Phys. Rev. Lett. **65**, 3173 (1990).
[49] Y. J. Uemura, A. Keren, K. Kojima, L. P. Le, G. M. Luke, W. D. Wu, Y. Ajiro, T. Asano, Y. Kuriyama, M. Mekata, et al., Phys. Rev. Lett. **73**, 3306 (1994).
[50] B. Martínez, F. Sandiumenge, A. Rouco, A. Labarta,

J. Rodríguez-Carvajal, M. Tovar, M. T. Causa, S. Galí, and X. Obradors, Phys. Rev. B **46**, 10786 (1992).

[51] C. Mondelli et al., *private communication*.

[52] A. P. Ramirez, Annu. Rev. Mater. Sci. **24**, 453 (1994).

[53] A. Keren, P. Mendels, M. Horvatić, F. Ferrer, Y. J. Uemura, M. Mekata, and T. Asano, Phys. Rev. B **57**, 10745 (1998).

[54] P. Mendels, A. Keren, L. Limot, M. Mekata, G. Collin, and M. Horvatić, Phys. Rev. Lett. **85**, 3496 (2000).

[55] L. Limot, P. Mendels, G. Collin, C. Mondelli, H. Mutka, and N. Blanchard, Can. J. Phys. **79**, 1393 (2001).

[56] D. Bono, P. Mendels, G. Collin, and N. Blanchard, J. Phys.: Condens. Matter **16**, S817 (2004).

[57] A. Keren, Y. J. Uemura, G. Luke, P. Mendels, M. Mekata, and T. Asano, Phys. Rev. Lett. **84**, 3450 (2000).

[58] D. Bono, P. Mendels, G. Collin, N. Blanchard, F. Bert, A. Amato, C. Baines, and A. D. Hillier, Phys. Rev. Lett. **93** (2004).

[59] D. E. MacLaughlin and H. Alloul, Phys. Rev. Lett. **36**, 1158 (1976).

[60] A. B. Harris, C. Kallin, and A. J. Berlinsky, Phys. Rev. B **45**, 2899 (1992).

[61] K. Motida and S. Miyahara, J. Phys. Soc. Jpn. **28**, 1188 (1970).

[62] E. J. Samuelsen, M. T. Hutchings, and G. Shirane, Physica **48**, 13 (1970).

[63] C. Mondelli, K. Andersen, H. Mutka, C. Payen, and B. Frick, Physica B **267-268**, 139 (1999).

[64] A. J. Garcia-Adeva and D. L. Huber, Phys. Rev. B **63**, 174433 (2001).

[65] P. Schiffer and I. Daruka, Phys. Rev. B **56**, 13712 (1997).

[66] M. Takigawa, N. Motoyama, H. Eisaki, and S. Uchida, Phys. Rev. B **55**, 14129 (1999).

[67] F. Tedoldi, R. Santachiara, and M. Horvatic, Phys. Rev. Lett. **83**, 412 (1999).

[68] M. Azuma, Z. Hiroi, M. Takano, K. Ishida, and Y. Kitaoka, Phys. Rev. Lett. **73**, 3463 (1994).

[69] S. Ouazi, J. Bobroff, H. Alloul, and W. A. MacFarlane, Phys. Rev. B **70**, 104515 (2004).

[70] R. Moessner and A. J. Berlinsky, Phys. Rev. Lett. **83**, 3293 (1999).

[71] A. Abragam, *Principles of Nuclear Magnetism* (Clarendon Press-Oxford, 1961).

[72] S. L. Lee, S. H. Kilcoyne, and R. Cywinski, eds., *Muon Science – Muons in Physics, Chemistry and Materials* (Scottish Universities Summer School in Physics & Institute of Physics Publishing, Bristol and Philadelphia, 1999), proceedings of the Fifty First Scottish Universities Summer School in Physics, August 1998.

[73] R. S. Hayano, Y. J. Uemura, J. Imazato, N. Nishida, T. Yamazaki, and R. Kubo, Phys. Rev. B **20**, 850 (1979).

[74] Y. J. Uemura, T. Yamazaki, D. R. Harshman, M. Senba, and E. J. Ansaldo, Phys. Rev. B **31**, 546 (1985).

[75] A. Keren, Phys. Rev. B **50**, 10039 (1994).

[76] A. Keren, K. Kojima, L. P. Le, G. M. Luke, W. D. Wu, Y. J. Uemura, M. Takano, H. Dabkowska, and M. J. P. Gingras, Phys. Rev. B **53**, 2451 (1996).

[77] A. Fukaya, Y. Fudamoto, I. M. Gat, T. Ito, M. I. Larkin, A. T. Savici, Y. J. Uemura, P. P. Kyriakou, G. M. Luke, M. T. Rovers, et al., Phys. Rev. Lett. **91**, 207603 (2003).

[78] K. Kojima, A. Keren, L. P. Le, G. M. Luke, B. Nachumi, W. D. Wu, Y. J. Uemura, K. Kiyono, S. Miyasaka, H. Takagi, et al., Phys. Rev. Lett. **74**, 3471 (1995).

[79] A. Chubukov, Phys. Rev. Lett. **69**, 832 (1992).

[80] F. Mila and D. Dean, Eur. Phys. J. B **26**, 301 (2002).

[81] M. Ferrero, F. Becca, and F. Mila, Phys. Rev. B **68**, 214431 (2003).

[82] Z. Hiroi, M. Hanawa, N. Kobayashi, M. Nohara, H. Takagi, Y. Kato, and M. Takigawa, J. Phys. Soc. Jpn. **70**, 3377 (2001).

[83] F. Bert, D. Bono, P. Mendels, J. C. Trombe, P. Millet, A. Amato, C. Baines, and A. Hillier, J. Phys.: Condens. Matter **16**, S829 (2004).

[84] K. Kojima, Ph.D. thesis, The University of Tokyo (1995).

[85] B. Ammon and M. Imada, Phys. Rev. Lett. **85**, 1056 (2000).

[86] A. Fukaya, Y. Fudamoto, I. M. Gat, T. Ito, M. I. Larkin, A. T. Savici, Y. J. Uemura, P. P. Kyriakou, G. M. Luke, M. T. Rovers, et al., Physica B **326**, 446 (2003).

[87] H. Kageyama, K. Yoshimura, R. Stern, N. V. Mushnikov, K. Onizuka, M. Kato, K. Kosuge, C. P. Slichter, T. Goto, and Y. Ueda, Phys. Rev. Lett. **82**, 3168 (1999).

[88] K. Kodama, M. Takigawa, M. Horvatić, C. Berthier, H. Kageyama, Y. Ueda, S. Miyahara, F. Becca, and F. Mila, Science **298**, 395 (2002).

[89] H. Mutka *et al.*, in preparation.

[90] M. H. Cohen and F. Reif, Solid State Physics **5**, 321 (1957).

[91] R. E. Walstedt and L. R. Walker, Phys. Rev. B **9**, 4857 (1974).

[92] J. H. Brewer, R. F. Kiefl, J. F. Carolan, P. Dosanjh, W. N. Hardy, S. R. Kreitzman, Q. Li, T. M. Riseman, P. Schleger, H. Zhou, et al., Hyperfine Interact. **63**, 177 (1990).

[93] This is different to the situation encountered in spin glasses, where the cooling history finishes by selecting one of the numerous local minima present in the free energy.

[94] We define the hamiltonian as $\mathcal{H} = J \sum_{\langle i,j \rangle} \mathbf{S_i} \cdot \mathbf{S_j}$ where i, j are the nearest neighbors.

[95] The $S = \frac{3}{2}$ Cr jarosite is the only exception [76].

[96] The official labelling are the following for SCGO [BSZCGO]: Ga(4f) [Ga(2d)] for Ga(1), Ga(4e) [Ga(2c)] for Ga(2), Cr(1a) [Cr(2a)] for Cr(a), Cr(12k) [Cr(6i)] for Cr(b) and Cr(4f$_{vi}$) for Cr(c) in SCGO. We used simplified notations for clarity in the comparison of both systems.

[97] Since the Ga(2) line of BSZCGO is governed by quadrupolar effects, its width is $\propto \nu_Q^2/\nu_l$ [90]. Therefore this line is broader at low field. On the contrary, the quadrupolar frequency of the Ga(1) is smaller and the linewidth is proportional to the applied external field.

[98] Notice that the high temperature analysis of both ^{71}Ga(1) and ^{71}Ga(2) lines in BSZCGO allows us to compare their shifts, which yields an estimate of the chemical shift of 0.15(3)%.

[99] We checked that the transverse relaxation time T_2 is homogeneous over the whole ^{71}Ga(2) line. Its shape is hence used for the subtraction whereas its intensity is multiplied by $\sim \exp[2(\tau_l - \tau_s)/T_{2,2}^{71}]$.

[100] In the case of SCGO, χ_{macro} is a three-component susceptibility, the third contribution coming from the Cr(c)-Cr(c) spin pairs, which we drop here for clarity.

[101] C. Lhuillier, Private communication.

[102] A dipolar broadening due to the diluted paramagnetic defects [91] would be to small to justify the broadening of the ^{69,71}Ga spectra.

[103] Ga(1) nuclei are coupled to 9 Cr(b) and 3 Cr(a). The measured susceptibility is hence $\chi_{\text{Kag,NMR}} \propto 9\chi_b + 3\chi_a$, where χ_b and χ_a are the Cr(b) and Cr(a) susceptibilities. On the other hand, the macroscopic susceptibility probes these susceptibilities with their stoichiometric ratio, i.e., $\chi_{\text{Kag,macro}} \propto 6\chi_b + \chi_a$ [55]. A small difference between the ratios χ_b/χ_a would yield a slightly different ratio $[\Delta H/H_l(p)]/C_{\text{def}}(p)$.

[104] We attribute the factor 8 between λ in both systems to a different coupling of the muon spin to the Cr spins. Transverse field experiments show for instance a larger linewidth in SCGO(0.95) than in BSZCGO(0.91) despite a lower defect term [41]. On the other hand, Δ, which is mainly created by dipolar interactions in μSR, is $\Delta \propto \sum 1/r^3$, where the sum is done over all the spins in the lattice and r is the distance between the muon site and these spins [73]. Usually, the muon is located near an O^{2-} ion [92]. In a very simplified approach, we computed Δ, considering that the muon would be located *on* the O^{2-} sites, as an average, and find $\Delta \approx 1100\ \mu s^{-1}$ and $800\ \mu s^{-1}$ in SCGO(1) and BSZCGO(1). This is in perfect agreement with the high temperature evaluation of Δ. Since $\lambda \propto \Delta^2$ in the fast fluctuation limit and $\lambda \propto \Delta$ in the static limit, we expect, with this simple approach, λ to be 1.5-2 times larger in SCGO(p). The missing factor 4 may either come from a more complex muon sites distribution, due to the O^{2-} ions around the Cr(c) sites, or to a different dynamics range as suggested by Neutron Spin Echo [89].

[105] According to us, no FC-ZFC magnetization data is published about $Sr(Cu_{1-x}Zn_x)_2(BO_3)_2$.